

NASA-TM-109,093

NASA Technical Memorandum 109093

NASA-TM-109093 19940028418



# **OARE Flight Maneuvers and Calibration Measurements on STS-58**

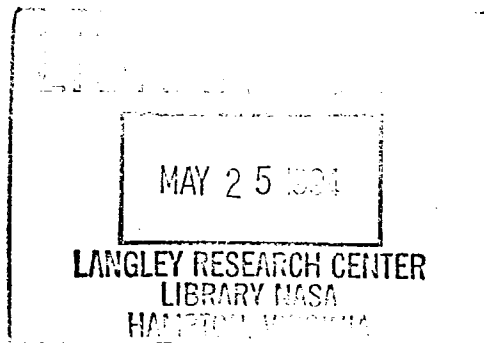
**R. C. Blanchard**  
*Langley Research Center, Hampton, Virginia*

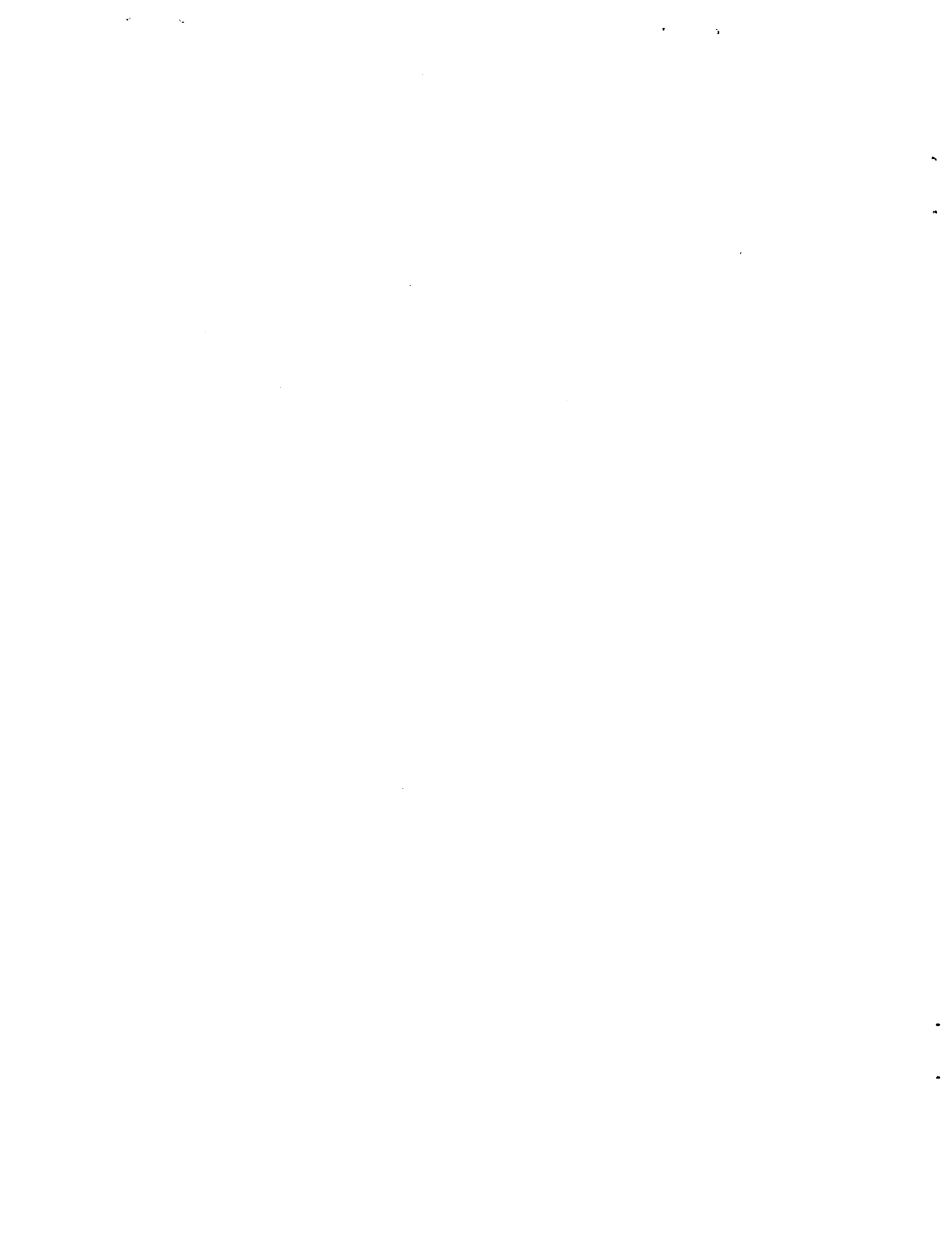
**J. Y. Nicholson**  
*ViGYAN, Inc., Hampton, Virginia*

**J. R. Ritter and K. T. Larman**  
*Lockheed Engineering & Sciences Co., Hampton, Virginia*

**April 1994**

National Aeronautics and  
Space Administration  
Langley Research Center  
Hampton, Virginia 23681-0001







# OARE Flight Maneuvers and Calibration Measurements on STS-58

Robert C. Blanchard  
NASA Langley Research Center  
Hampton, Virginia 23681-0001

John Y. Nicholson  
ViGYAN, Inc.  
Hampton, Virginia 23666-1325

James R. Ritter & Kevin T. Larman  
Lockheed Engineering & Sciences Co.  
Hampton, Virginia 23666-1339

## Abstract

The Orbital Acceleration Research Experiment (OARE), which has flown on STS-40, STS-50 and STS-58, contains a 3 axis accelerometer with a single, non-pendulous, electrostatically suspended proofmass which can resolve accelerations to the nano-g ( $10^{-9}$  g) level. The experiment also contains a full calibration station to permit *insitu* bias and scale factor calibration. This on-orbit calibration capability eliminates the large uncertainty of ground-based calibrations encountered with accelerometers flown in the past on the Orbiter, thus providing absolute acceleration measurement accuracy heretofore unachievable. This is the first time accelerometer scale factor measurements have been performed on orbit. A detailed analysis of the calibration process is given along with results of the calibration factors from the on-orbit OARE flight measurements on STS-58. In addition, the analysis of OARE flight maneuver data used to validate the scale factor measurements in the sensor's most sensitive range is also presented. Estimates on calibration uncertainties are discussed. This provides bounds on the STS-58 absolute acceleration measurements for future applications.

## Nomenclature

A	acceleration component
<b>A</b>	acceleration vector
B	bias
C	aerodynamic coefficient
$C_A$	axial coefficient
$C_N$	normal coefficient
$C_Y$	side force coefficient
g	gravitational acceleration (9.80665 m/s <sup>2</sup> )
$K_0$	conversion factor ( 1.05 x 10 <sup>5</sup> $\mu\text{g}/\text{m}/\text{s}^2$ )
$k_\tau$	acceleration per unit length for gravity gradient effect
$k'_\tau$	acceleration per unit length for out of plane effect
M	Orbiter mass
micro-g	$\mu\text{g}$
nano-g	ng
p,q,r	body rates
$\dot{p},\dot{q},\dot{r}$	body angular accelerations
<b>r</b>	distance vector
$\mathbf{r}_s$	OARE location vector in Orbiter
$\mathbf{R}_s$	OARE proofmass location on table
$S_{\text{ref}}$	aerodynamic reference area
S	bias free signal
SF	scale factor ratio, see equation (1)
T	body to sensor transformation matrix
$V_a$	air relative velocity
$\mathbf{V}_a$	air relative velocity vector
X, Y, Z	sensor, body, or Orbiter axes
$\hat{x},\hat{y},\hat{z},\hat{r}$	unit vectors
$\alpha$	angle of attack
$\beta$	side-slip angle
$\Delta h$	vertical change in altitude
$\theta_a,\theta_b,\theta_c$	angle between Orbiter axes and radius vector
$\phi_a,\phi_b,\phi_c$	angle between OARE sensor and radius vector
$\rho$	atmospheric density
$\omega$	body rate magnitude
$\boldsymbol{\omega}$	body rate vector
$\boldsymbol{\omega}_s$	calibration table rotation rate vector
$\dot{\boldsymbol{\omega}}$	angular acceleration vector
ng	1 x 10 <sup>-9</sup> g
$\mu\text{g}$	1 x 10 <sup>-6</sup> g

### *subscripts*

a	axial direction
aero	aerodynamic components
b	body axes
gg	gravity gradient components
h	horizontal component
o	Orbiter reference axes
n	normal direction
oop	out-of-plane components
r	along radius
s	refers to sensor
theor	theoretical
x,y,z	refer to x, y, and z axes, respectively
0,180	angle positions of 0° and 180°

### *Acronyms*

ACIP	Aerodynamic Coefficient Identification Package
HiRAP	High Resolution Accelerometer Package
GSE	Ground Support Equipment
JSC	Johnson Space Center
LRU	Line Replaceable Unit
MET	Mission Elapsed Time
OARE	Orbital Acceleration Research Experiment
ODRC	Orbiter Data Reduction Complex
OEX	Orbiter Experiment
STS	Shuttle Transportation System

## Introduction

The Orbital Acceleration Research Experiment<sup>1</sup> (OARE) contains a tri-axial accelerometer which uses a single free-floating (non-pendulous) electrostatically suspended cylindrical proofmass. The accelerometer sensor assembly is mounted to a microprocessor-controlled, dual-gimbal platform in order to perform in-flight calibrations. Acceleration measurements are processed and stored in the OARE flight computer memory and, simultaneously, the unprocessed data are recorded on the shuttle payload tape recorder. This payload tape recorder data are telemetered periodically to ground stations during flight. The OARE is the third-generation Orbiter Experiment (OEX) Program accelerometer package. Its capabilities exceed both the Aerodynamic Coefficient Identification Package<sup>2</sup> (ACIP)\* and the High Resolution Accelerometer Package<sup>3</sup> (HiRAP)\*\* in sensitivity and performance.

OARE's objective is to measure Orbiter aerodynamic performance on orbit and thus is purposely designed for low-frequency signals only. As the low-frequency acceleration environment of the Orbiter contains a variety of components, measurements or models of these components embedded in the acceleration measurements are required in order to extract the orbiter aerodynamic acceleration signal. The models and measurements required to separate the components of low-frequency acceleration are discussed in the appendix in this report.

There are several features which make the OARE desirable for making low-frequency acceleration measurements. One unique design feature of the OARE equipment is its capability to perform both bias and scale factor calibrations on orbit. The OARE is the first accelerometer flight equipment to use in-flight scale factor capabilities. Another experiment design feature is the OARE sensor which is a non-pendulous type accelerometer. Pendulous accelerometers, such as HiRAP, do not readily lend themselves to calibration on orbit because they are highly temperature sensitive in the micro-g ( $\mu\text{g}$ ) range. In the past, pendulous accelerometers have depended upon ground calibrations. Experience has shown ground calibration to be unreliable in predicting absolute bias on orbit.<sup>4</sup> Consequently, these accelerometers are unable to measure absolute acceleration signals with predictable accuracy. Therefore, OARE stands alone in its ability to establish precise absolute accelerations on orbit. Such measurements, in addition to extracting Orbiter rarefied-flow aerodynamic performance, are also crucial in characterizing the low-frequency

---

\* ACIP has flown on all OV-099 and OV-102 flights (Challenger and Columbia respectively). The ACIP sensor best resolution is 61  $\mu\text{g}$ s on the lateral axis channel.

\*\* The High Resolution Accelerometer Package (HiRAP) is a sensitive pendulous triaxial accelerometer package interfaced to the ACIP system. HiRAP has flown on all OV-099 and OV-102 flights subsequent to STS-5. The HiRAP accelerometers have a resolution of 1  $\mu\text{g}$ , with  $\pm 5 \mu\text{g}$  accuracy.

environment for many experiments on the Orbiter, such as those involving electrophoresis, diffusion, and crystal growth.<sup>5</sup> These experiments are being performed by a variety of national and international researchers.<sup>6,7,8</sup> The need to know the Orbiter vehicle microgravity environment is documented in the literature.<sup>5,9</sup>

The initial developmental flight of the OARE equipment was in June 1991 on Shuttle mission STS-40.<sup>10</sup> This was followed by a second developmental flight, STS-50, in July and August of 1992.<sup>11</sup> The OARE was flown a third time during August 1993 on Shuttle mission STS-58. This paper provides an indepth discussion and analysis of the bias and scale factor calibrations performed during the orbital portion of this flight. The report concentrates on biases and scale factors for only the most sensitive instrument range since this is the applicable range while in orbit. In addition, this report provides the analysis of the three sets of flight maneuvers and the extraction of the scale factors for each axis from these maneuvers.

### **Coordinate Systems**

Three coordinate systems are used in this report. Figure 1 shows schematically the three coordinate systems in relation to one another. The OARE coordinate system (X,Y,Z) corresponds to the input axes of the OARE sensor and the center of the system is at the center of the proofmass. Positive X acceleration is toward the nose of the Orbiter, while positive Y acceleration is through the top of the fuselage of the Orbiter. Positive Z is out the right wing. Use is made of the standard aircraft body axis system ( $X_b, Y_b, Z_b$ ) whose center is located at the Orbiter's center of gravity. Positive  $X_b$  is toward the nose, positive  $Y_b$  is out the right wing, and positive  $Z_b$  is toward the bottom of the orbiter fuselage. The Orbiter reference system ( $X_o, Y_o, Z_o$ ) is also used since this coordinate system is used by the Orbiter Project to locate objects in or attached to the Orbiter. As shown on Fig. 1, the center of this system is located 235 in. in front of the nose of the Orbiter and about 400 in. down from the fuselage outer mold line.<sup>12</sup> (Units of inches are used in accordance with accepted Shuttle Project Office practices with this coordinate system.) Positive  $X_o$  is toward the aft of the vehicle,  $Y_o$  is out the right wing, and  $Z_o$  is through the top of the fuselage.

### **Instrument Overview**

Figure 2 is a schematic of OARE, showing the various instrument components. The package is 43.2 x 33 x 104.1 cm (17 x 13 x 41 in.) and is mounted on a keel bridge at bay 11 on the cargo bay floor. The OARE sensor axes are co-aligned with the Orbiter body axes as shown on Fig. 1. The instrument weighs 53.2 kg (117 lbs) and requires 110 watts of power. Three line replaceable units (LRU) are mounted to a keel bridge mounting plate. The three LRU's consist of: (1) the calibration table and sensor package, (2) the interface electronics, power system and servo control modules, and (3) the 16-bit programmable micro-computer and memory. The

accelerometer sensor (labeled sensor package in Figs. 2 and 3) is attached to a moveable platform. The platform is rotated about two axes by two brushless DC torque motors.

Table 1 provides the sensor ranges, resolutions and scale factor calibration signals. There are 3 sensor ranges, A, B, and C, which correspond to acceleration scales for the X-axis of  $\pm 10,000$ ,  $\pm 1000$  and  $\pm 100$   $\mu\text{g}$  respectively. The Y- and Z-axes are slightly different from X due to the proofmass cylindrical design. The resolution in each axis and range is also given in Table 1. The best resolution of the sensor is  $3.05 \times 10^{-9}$  g which is along the X-axis. Table 1 also shows the scale factor calibration signals which range from 20 to 1392  $\mu\text{g}$  depending upon the table angular rate. There are two rates per range to check sensor linearity. In addition, the calibration platform moves in two angular directions, forward and reverse, for each axis of rotation in order to resolve platform motion characteristics.

## **In-flight Calibration**

### **Calibration Station Overview**

OARE bias and scale factor calibration data are acquired in flight using a computer-controlled, dual-gimbal rotary platform, referred to as the calibration station. A sketch of the OARE Calibration Table Assembly is shown in Fig. 3. This element is one of the OARE LRUs briefly discussed earlier and shown in Fig. 2. The inner gimbal motor moves the sensor package attached to the platform around the inner gimbal axis to stimulate the X-axis sensor or to locate the sensor input axis in a desired direction. This is accomplished using a 16-bit optical encoder to control the platform position. Known acceleration signals can be generated to determine scale factors simply by rotating the platform at a known constant rate. In addition, biases can be determined by locating the input axis in  $180^\circ$  opposing directions, similar to a dividing-head used in most accelerometer calibration laboratories. The outer gimbal motor provides a similar function for the Y- and Z- axes. Both of these input axes are simultaneously stimulated during rotation about the outer gimbal axis.

### **Calibration Process**

The OARE sensor, like all accelerometers, is affected by manufacturing tolerances and variances in physical environment including temperature and humidity, by its own inherent electronic drift, and by degradation of electronic components over time. These all impose a slowly changing acceleration signal. Because of this, periodic bias and scale factor determinations are required to assure instrument accuracy.

Prior to flight, the bias and scale factor measurements are scheduled at definite time intervals. Together, the biases and scale factors determined from the measurements are used to obtain an absolute reference for the measured signal. Bias determination is handled through scheduled reorientations of the sensor, and scale factor calibrations are handled

through rate-controlled rotations. The bias measurement accounts for instrument offset measured when no signal is present; the scale factor provides a means to scale the output signal across the measurement range of the instrument. Since OARE has three measurement ranges, biases and scale factors are determined for each of the A, B, and C ranges for each of the three axes. The number of biases recorded for each axis and each range during STS-58 is given in the following table:

RANGE	X-AXIS	Y-AXIS	Z-AXIS
A	70	62	70
B	69	68	70
C	71	70	70

There were 87 scale factor calibrations recorded for each of these nine cases.

The following two sections provide a general description of the bias and scale factor process.

### **BIASES**

An example of the OARE bias process using the X-axis is shown schematically in Fig. 4. The sensor proofmass is shown mounted on the table, offset from the inner gimbal axis as shown in the Figure. Sketch A shows the orientation of the input axis at the reference position, 0°. The bias is measured by rotating the sensor 180°, shown in sketch B, and comparing the measurements made at 0°. The sum of these measurements yield twice the bias, while the difference is twice the input signal, as indicated in the figure. Repeating this process for rotations around the outer gimble axis provides bias data for the Y and Z-axes. In flight, the total bias calibration takes 8 to 10 minutes (3 axes, 3 ranges) and is performed periodically throughout the mission. A set of 500 data points are collected in each position for each axis for each range. The bias measurements are processed in-flight by the programmable micro-computer and stored in the onboard OARE memory.

The basic assumption in this process is that during the bias measurements the input signal,  $S_x$ , does not change appreciably. In the laboratory this can be closely controlled, but not on the Orbiter. In lieu of this, certain experimental steps can be taken to minimize the errors introduced into the process. For example, by keeping the measurement time frame small, by taking a statistically significant sample, and by monitoring the Orbiter movements, the errors introduced can be kept small enough to meet the experiment objectives. This is discussed in a later section.

## SCALE FACTORS

A typical OARE scale factor process for the Y and Z-axes is shown schematically in Fig. 5. Each of these axes lies in a plane perpendicular to the outer gimbal axis and at a 45 degree angle from the radius vector (outer gimbal axis) to the sensor. Depicted is the sensor proofmass and table viewed along the outer gimbal axis looking forward in the orbiter. The sensor proofmass is offset from the rotation center of the table such that a steady table rotation ( $\omega$ ) around the outer gimbal axis produces a known input acceleration into the sensors. By rotating the table at two different rates per range, the linearity of the sensors in the Y and Z-axes directions can be examined. The instrument is designed to be linear over each range. Repeating this process for rotations around the inner gimbal axis provides scale factor data for the X-axis. The length of time for the rotation process and the induced centripetal calibration acceleration signals are given in Table 1.

### **Calibration Sequence**

A typical OARE flight calibration sequence for both biases and scale factors is shown in Fig. 6 as a function of gimble angle measurements versus mission elapsed time (MET). This is a typical half hour calibration segment during which the measurements for the biases and the scale factors for the 3 axes and the 3 ranges are performed. On STS-58, 43 complete sequences were collected.

## BIAS SEQUENCE

The range sequence for the bias measurements is C-, B-, and then A. That is, the sensor is progressively forced to the higher scales, starting with the most sensitive range (C) which is the typical range for on-orbit acceleration measurements. For the bias measurements in a given range, data are first collected in the (0,0) gimbal reference position. Then the outer gimbal is changed by 180° and data are collected for the Y- and Z- axes. Data are simultaneously collected for the X axis in its normal position. The outer gimbal axis is brought back to reference, the inner gimbal is moved 180°, and data are then collected for the X-axis. Six sets of processed data are recorded in memory, i.e., data sets for normal and opposite positions for all three axes. Subsequently, the sensor is placed back at the reference gimbal position and the process is repeated for the other two ranges. Thrustor firings, mechanical subsystem activities, spacecraft maneuvers, satellite launches, as well as other experiment activities in the Orbiter will affect the measurements.

## **SCALE FACTOR SEQUENCE**

The scale factor flight sequence also starts with the C-range, and then moves to B-, and then A-range. In a given range the inner gimbal is moved to a mid-position of its traveling range and data are collected for the scale factor reference calculation. The platform is moved to its extreme motion limit and then rotated at a constant fixed rate. Data are collected while the sensor is in motion. Next, the sensor is moved back to its mid-position and another set of data are collected.

The complex table motion sequence is best illustrated by considering the data collection process for the X-axis in the C-range. The corresponding gimble angles are given in Fig. 6. First, the sensor is moved to a position halfway through its preprogrammed slew. For example, the C range, low rate slew for generating scale factor calibration data requires the X axis to travel from inner-gimbal angle of  $+150^{\circ}$  to  $-60^{\circ}$  at a rate of 0.0970 radians/second (37.8 seconds). Thus, the sensor is moved to the mid-point position of  $+45^{\circ}$  and raw acceleration data are recorded for 32.2 sec. The table then moves to the inner-gimbal starting position of  $+150^{\circ}$  and slews at the prescribed rate until  $-60^{\circ}$  is reached. This second set of acceleration data are recorded also for 32.2 seconds during this slew. Subsequent to this, the inner-gimbal angle is reset to mid-position and a third set of data are recorded. This sequence is performed again for the X-axis at a higher rate. (It is difficult to see the change in slope for the higher rate in Fig. 6 due to the choice of graphing scales.) The process is repeated for the Y- and Z-axes by holding the inner gimbal angle at zero while changing the outer gimbal angle.

Once the data have been collected for the 3 axes in the C-range for the 2 rates, the whole process is repeated for the B- and A- range as indicated in Fig. 6. Unlike the bias data, the data collected for scale factor calculations is not processed in flight. The example shown in Fig. 6 is for a reverse direction platform motion. Throughout the mission, the platform is alternately rotated in the opposite direction producing forward direction scale factors. Alternate table directions provide a means to check table tolerances.

### **Bias Calibration Results**

During the STS-58 mission, the root-mean-squared noise of the acceleration signals is about 2 to 4  $\mu\text{g}$  for "quiet" times to well above 10  $\mu\text{g}$  for "active" times. Active times occur during crew work periods when life support systems are active, the crew is involved in experiments, small thrusters are fired, etc. To extract information in this environment, a statistical "trimmed-mean" filter is used on the measurements taken during the bias calibration.<sup>10</sup> In orbit, the "trimmed-mean" averaged signals are recorded in the OARE computer memory, along with their

statistics (1-sigma deviations), the MET, and sensor temperature. Generally, the greatest contributor to the magnitude of the 1-sigma deviations come from the environment.

The results of these STS-58 OARE measured biases for the X, Y, and Z-axes, along with their respective error bars, are shown in Fig. 7 and can be compared with the results from STS-50 shown in Fig. 8. The Y and Z axes show an apparent improvement in errors, but this is only the result of an electronic filter change for the STS-58 mission. The errors on the X-axis appear significantly larger on STS-58. This is surprising since the STS-50 mission had the more rigorous schedule (i.e., red/blue teams working experiments around the clock). More significantly, however, the X-axis has clearly shifted from a negative (STS-50) to a positive (STS-58) bias.

In both Figs. 7 and 8 a noticeable bias drift in all axes occurs at the beginning of each mission for about 40 to 50 hours, after which it remains fairly constant. This is due to dielectric charging of the ceramic forcer ring assembly and is a characteristic of the sensor.<sup>13</sup> The drift is most pronounced on the X-axis which is furthest from the sensor's internal discharge path.

The temperature sensitivity of the biases for both flights can be seen in Fig. 9. This figure shows clearly the very low bias temperature sensitivity of the sensor, thus providing an ideal situation for low-frequency acceleration measurements. Of interest in showing the comparison of the data between two flights is the long term behavior. These flights are separated by many months and the instrument is subjected to severe launch and landing shock, vacuum to sea level pressure changes, and other severe environmental changes such as temperature and humidity. The only significant change in the bias behavior is for the X-axis. Its bias and temperature dependence have changed whereas very little change can be seen for the Y- and Z-axes when comparing STS-58 to STS-50. This change in the X-axis is probably influenced by the eminent failure of the operations amplifier circuit. This failure occurred after STS-58 data collection was completed and was discovered after the instrument was removed from the Orbiter. In general, however, this poses no serious problems for further interpretation of absolute acceleration levels for either flight since the bias behavior is measured frequently throughout both missions.

## Scale Factor Calibration Results

As discussed, the on-orbit scale factor calibration of each sensor axis is accomplished by rotating the proofmass at known rates about one of the two gimbal axes (i.e., the inner-gimbal axis for X-axis calibration and outer-gimbal axis for Y/Z-axes calibration). The distances from gimbal axes to proofmass are known precisely and the rotation rates are accurately controlled; thus, the calibration acceleration signal can be calculated within a fraction of one percent. This calibration input signal is referred to as the "theoretical" signal.

In principle, the reference value obtained when the sensor is not rotating is subtracted from the measured acceleration during rotation.

This difference provides the relative acceleration amplitude generated by the platform motion. This amplitude, referred to as the "measured" acceleration, is compared to the theoretical acceleration to define the scale factor ratio, SF, that is,

$$SF = A_{\text{theor}}/A_{\text{meas}} \quad (1)$$

The scale factor ratio typically has a value near unity. This would be the situation if the counts from the accelerometer, which are initially "scaled" on each range using the manufacturer conversion factors, correspond exactly to the theoretical signal produced by the platform rotation. The SF is used as a multiplier adjustment to the acceleration measurements made during flight after subtracting the bias.

The reference signal is measured at rest at a position half way through the slew. This reference, therefore, should eliminate all but a small amount of the effects of outside residual acceleration on the determination of the scale factor ratio. However, these external accelerations, mainly from gravity-gradient and out-of-plane effects, Orbiter rotation, and Coriolis acceleration from simultaneous Orbiter rotation and platform slew rotation, are calculated and are found to alter the scale factor by about two percent in some cases. These effects have been incorporated in the scale factor data reduction process.

Each range (A, B, or C) for each axis employs a low and a high rate slew which are used to determine the extent that the scale factor varies with acceleration level. In addition, the slew can be forward or reverse rotation. This direction is recorded for each scale factor determination so that any direction-dependent effect can be identified.

Figures 10 and 11 are the results of the scale factors measurements for the X and Y-axes, C range for STS-58. Note that, in the X axis case, forward and reverse slews have very little effect on the magnitude of the scale factor, but the scale factor does increase slightly from low to high rate, which may indicate a slight nonlinearity. The Y axis scale factor changes very little with slew rate, but does appear to decrease slightly throughout the flight for both rates.

For STS-58, the Z-axis did not perform properly in the C range during its scale factor induced motion. Post-flight diagnostics indicate that saturation of the signal conditioner caused by a "jitter" of the motor corrupted the Z-axis signal in the C range. This required a special analysis to recover the scale factor for this axis. The analysis and the results are discussed next.

### **Z-AXIS SCALE FACTOR ANALYSIS**

In general, the forward direction low and high rate platform motion did not produce the expected acceleration pulse during the Z-axis scale factor data accumulation for the entire flight. Both low and high rate signal characteristic was that of a sawtooth wave with no clearly

discernible horizontal at-rate level. Figures 12 and 13 provide an illustration of the type of data obtained during the STS-58 mission for the low and high rate table motion, respectively. However, the reverse direction low and high rate data almost produced the anticipated acceleration pulse. Figures 14 and 15 provide an illustration of the typical signals during the accumulation of data for the Z-axis during reverse direction of the platform. Clearly, this is not the typical square wave pulse expected. But, it is possible to glean some information from these signals. Thus, only the reverse direction low-and high-rate Z-axis data were used to calculate Z-axis scale factors. Further, the calibration measurement sets utilized were taken during the relatively low background acceleration disturbance which occurred when the astronauts slept.

In addition to the ill-defined pulse signal shown in Figs. 14 and 15, the pre and post at-rate data segments exhibited characteristics of an instrument electronic bias in that these magnitudes flipped between two discreet magnitudes instead of the expected single nominal value. The true measured value must be adjusted for this electronic bias. The electronic bias is calculated by determining the difference between the forward, high rate, post-slew magnitude Fig. 13 and the subsequent reverse, low rate, pre-slew magnitude Fig. 14. This difference is added to the nominal measured value of both the reverse low Fig 14 and high rate Fig. 15 values to form the true measured at-rate values used to calculate the scale factors. As with the X and Y-axes, the nominal measured acceleration value is the difference between the at-rate magnitude and the average of the pre- and post-rate magnitudes. The scale factors determined from the low and high rate angular velocity are presented in Fig. 16. The mean scale factor for the reverse low rate is 1.11 and for the reverse high rate is 1.17.

### **In-Flight Calibration Maneuvers**

The stimulus to an accelerometer for acquiring data to measure the scale factor is usually accomplished by mounting the sensor to a moveable platform and rotating it in a controlled fashion. Some laboratories use a centrifuge device for this purpose. This activity is accomplished in orbit with high accuracy using the OARE calibration table, as previously discussed. It can also be accomplished by holding the calibration station at rest and rotating the spacecraft itself at prescribed, measureable rates.

One of the experiment goals of the OARE is to provide validation information of the scale factor data generated by the calibration table, since this is the first attempt to perform scale factor measurements in space. A series of orbiter flight maneuvers were designed in order to stimulate the OARE sensor axes in a predictable manner, in order to validate the calibration station. These Orbiter maneuvers consisted of a series of three, 360° rotations (i.e., pitch, yaw, and roll) about each of its body axes. A schematic of the maneuvers is presented in Fig. 17. On STS-58, three sets of these maneuvers were performed during the mission on MET days 2, 6, and 9. This section reports on the analysis and results from these maneuvers.

## Maneuver Analysis

In principle, spacecraft rotation imitates the OARE calibration station scale factor calibration activity, but there are significant differences in the way the measurements are analyzed. First, during spacecraft rotation, the OARE instrument encounters changes in aerodynamic and gravitational stimuli. These stimuli must be identified and accounted for in the theoretical signal before scale factor calculations can be made (e.g. see Appendix for details). These stimuli, as well as inertial coupling, produce small derivatives of the rotation rates which in turn also affect the theoretical acceleration.

To generate the calibration signal (referred to earlier as the "theoretical" signal) by rotating the spacecraft, the components of the calibration signal are calculated using measurements taken from the Orbiter Data Reduction Complex (ODRC) at JSC. The vector equation for the theoretical signal is,

$$\mathbf{A}_{\text{theor}} = \mathbf{A}_{\text{aero}} + \mathbf{A}_{\text{gg}} + \mathbf{A}_{\text{oop}} + \boldsymbol{\omega} \times \boldsymbol{\omega} \times \mathbf{r} + \dot{\boldsymbol{\omega}} \times \mathbf{r} \quad (2)$$

These components of the signal include aerodynamic, gravity-gradient and out-of-plane terms, and terms involving angular rates and accelerations about the Orbiter center-of-gravity. The position of the OARE proofmass center of gravity within the spacecraft is accurately known from measurements taken during initial installation in the Orbiter. (In the Orbiter coordinate system,  $X_0=1153.140$  in.,  $Y_0=-1.313$  in., and  $Z_0=317.932$  in.) The Orbiter center-of-gravity in the Orbiter coordinate system as a function of mission elapsed time is provided by the Orbiter Project Office. The difference in these two locations establishes  $\mathbf{r}$  in the above equation as a function of mission elapsed time. The rotational accelerations,  $\dot{\boldsymbol{\omega}}$  (i.e., body rate derivatives) are defined from piecewise curve fitting and differentiation of  $\boldsymbol{\omega}$  for selected data segments. Equation (2) is used to produce the theoretical calibration signals to which the OARE measurements are scaled.

An example of an intermediate step to the final scale factor results is given in Fig. 18 which shows the OARE measured acceleration components along the  $X_b, Y_b,$  and  $Z_b$  body axes during the third maneuver. The set of maneuvers typically lasts about 0.5 h. The OARE measurements shown contain no bias correction and nominal (SF=1) scale factor values. The predicted (theoretical) accelerations shown are for regions in which  $\dot{\boldsymbol{\omega}}$  was determined with sufficient accuracy from the gyro measurements. The  $\boldsymbol{\omega}$  components i.e., p,q,r (rotations about  $X_b, Y_b,$  and  $Z_b$  respectively) are shown in Fig. 19 for the entire maneuver sequence. The rates of each reach approximately 1 deg/s during the three maneuvers. The presence of derivatives of p, q, and r are easily inferred from Fig. 19; the need for accurate angular accelerations is apparent.

After removing the bias from the measured accelerations in Fig. 18, the scale factor can be determined in a least-square process. Figure 20 shows the same predicted data given in Fig. 18. The measurements in Fig. 20 are the results after adjusting for the instrument bias and solving for the scale factor on each axis. The match between the measurements and the predictions are excellent, as can be seen in the figure. A summary of all the calculations and solutions for scale factor from the three maneuvers is given next.

### Scale Factor Results

In general, for an accelerometer not on the vehicle center of gravity, the following table provides the axes in which scale factor solutions are possible as a function of spacecraft maneuver:

MANEUVER	AXIS ROTATE ABOUT	SCALE FACTOR SOLUTION AXIS
PITCH	Y	X * Z
YAW	Z	X Y *
ROLL	X	* Y Z

Each maneuver provides data for scale factor solutions for two axes. Thus, the three maneuvers give two scale factor solutions for each axis. Ideally, for a perfect instrument (i.e., no non-linearities or other aberrations), with perfect maneuvers (i.e., no cross coupling motions or angular accelerations), and error free angular measurements (i.e., perfect gyros), the solutions would be redundant. In fact, this is not the case, but the multiple solutions provide data upon which to judge the reliability of the solutions obtained. Mission STS-58 data are particularly unique because three sets of maneuvers were performed allowing six independent solutions per axis to be obtained.

Table 2 summarizes the data resulting from the analysis of the three maneuvers. The table has two parts, namely, Part (i), the scale factor results for all the maneuvers on STS-58 and Part (ii), the average induced accelerations along each axis at the OARE location which are generated by each of the three sets of maneuvers. The scale factor solution for the  $X_b$ -axis yields  $1.06 \pm .01$ . Comparing this to Fig. 10 (the calibration station scale factor) shows that on the average this value is larger by about 0.05 than the average scale factor measured over the entire mission.

There are two plausible explanations for these differences: (1) there is a slight non-linearity in this axis over its operating range, or (2) the center-of-gravity of the Orbiter is off (too far forward) by about 7.5 cm (~3 in.). The linearity argument does not appear to work since the acceleration induced in the X-axis during the high platform rate is very near the

acceleration created by the Orbiter yaw motion. Thus, it is highly likely that the tabular center-of-gravity location of the Orbiter is slightly in error. That is, a slight shift of the Orbiter center-of-gravity location about 3 in. aft would completely resolve the differences in scale factors between the maneuvers and the platform motion.

From Table 2, the scale factor solution for the  $Y_b$ -axis is  $1.075 \pm .05$  based upon the yaw maneuvers and  $0.81 \pm .2$  based upon the roll maneuvers. This compares with Fig. 16 (Z-sensor axis) calibration station scale factor value of  $1.14 \pm .03$ . The most reliable solution is 1.075 since the roll maneuvers did not stimulate the sensor much due to the proximity of the instrument to the center of rotation (see Table 2, Part ii ). Also, the values obtained from the calibration table are questionable since they come from a poor quality signal, as discussed earlier.

The scale factor solution for the  $Z_b$ -axis is  $1.11 \pm .01$  as determined from the maneuvers. This compares with Fig. 11 ( Y-sensor axis) average values throughout the mission of 1.14. This is quite close indicating that calibrations for this axis are quite reliable.

### **Uncertainty Bounds**

On-orbit bias and scale factor measurements provide the means to produce absolute acceleration measurements. However, both bias and scale factor determinations on orbit have uncertainties associated with them. For example, the instrument exhibits small variations, the conditions under which data are taken can be disturbed by spacecraft motion or from jets firing, and a limited set of measurements are taken as a matter of practicality. Thus, the determination of the absolute acceleration is known to within certain limits which are a direct function as to how well both the bias and scale factors have been determined. This section provides a separate summary of the estimates for each of these and, also, the estimates for maneuver errors.

### **BIAS ESTIMATES**

Figure 21 contains three graphs of the standard error along each of the OARE sensor axes for each of the bias measurements taken on STS-58. The standard error is calculated in the following manner. Each bias measurement contains two separate independent sets of measurements, one in a given direction and another  $180^\circ$  opposite to that direction. A trimmed-mean filter is applied to each set of these measurements separately resulting in a mean and a standard deviation. The average of the standard deviations is calculated and the Central Limit Theorem<sup>14</sup> is applied.

There are two average standard errors given on each graph in Fig. 21. The larger number is the statistic of using all 69 measurements, while the smaller number is obtained by using the values when the crew is asleep (these data are those with the filled in circles). This subset of measurements is of superior quality and is more indicative of the true capabilities of the OARE calibration system.

Finally, it is clear that the standard error is a function of the OARE internal electronic filters. The X-axis errors are three times larger than the Y/Z-axes. But this is due to the internal electronic smoothing process intentionally introduced in the Y/Z-axes to eliminate the platform jitter along these axes during scale factor activities.

### **SCALE FACTOR ESTIMATES**

Figure 22 contains three graphs of the standard error along each of the OARE sensor axes for each of the scale factor measurements take on STS-58. The standard error is calculated in the same manner as the bias standard error, with a few exceptions. First there are three sets of data per scale factor measurement, namely a set of measurements before, during, and after platform motion. Thus the average involves three standard deviations instead of two, as for the bias. The other consideration is that each Z-axis data set was individually inspected; data and entire sets were removed, thus affecting the statistics.

Again, examining Fig. 22, the quiet periods during astronauts sleep provide the ideal time to perform the calibration measurements. These data are indicated by the filled-in circles on each graph in the figure and the average is significantly smaller than the average taken over the entire mission. The X-axis errors are again significantly larger than those for both Y and Z-axes, a product of internal smoothing, as explained earlier.

### **ESTIMATES DURING MANEUVERS**

The errors associated with determining scale factors from the maneuvers are complex since they come from several sources, namely measurement errors (e.g. the body rates and angular accelerations, the center-of-gravity location, the sensor location) and model errors (e.g. the aerodynamic coefficients, density, angular orientations for gravity gradient effects). In lieu of a formal error analysis, this report provides an estimate of the error bounds by examining the variations in the scale factor solutions shown in Table 2. There are six scale factor solutions per axis, and the variations for the scale factor are  $\pm 0.01$ ,  $\pm 0.21$ , and  $\pm 0.01$  for the X-, Y-, and Z-axes, respectively. The Y-axis variation is the largest mainly due to the poor solutions during the roll maneuver (very short lever arm in this axis). Neglecting these solutions would provide a variation approximately equivalent to that obtained in the other two axes.

## Summary

The Orbital Acceleration Research Experiment (OARE), a tri-axial, electrostatically suspended, single proofmass, accelerometer system, with nano-g sensitivity and in-flight calibration capability has flown on STS-40, STS-50, and STS-58. The OARE microcomputer is preprogrammed to operate the calibration station in order to provide data for both bias and scale factor determinations. Bias data are processed inflight and stored in the OARE computer memory, while data generated for scale factor calculations are stored for post-flight processing.

Detailed analyses of both in-flight bias and scale factor measurements for STS-58 have been performed. Bias measurements collected during flight for 3 axes and 3 ranges are designated as C-, B-, and A-ranges, where the C-range in the X-axis is the most sensitive scale of the instrument ( $\pm 100 \mu\text{g}$ ). Scale factor data are collected for three axes, three ranges, and in addition, two platform rates, and two rotational directions. This report presents the analysis of the C-range data since this is the most applicable range while the Orbiter is in orbit.

On STS-58, the Y and Z axes bias results matched closely the data obtained on the previous flight, STS-50. The X-axis indicated a significant change between flights. But subsequent to the STS-58 mission, a major electronic component failed suggesting an influence in the operation of the sensor during that flight. In perspective, however, the Y/Z-axes bias results show no significant change in magnitude nor change in temperature sensitivity. This provides the first evidence of system robustness when subjected to shock, severe environment changes, and a considerable passage of time between flights.

The calibration station scale factor results on all three axes were obtained throughout the entire flight. However, there was a problem with the Z-axis due to jitter during platform motion which caused a significant deterioration of the results on this axis.

A detailed analysis of three sets of pitch, yaw, and roll maneuvers of the Orbiter were examined to verify the scale factor results which were determined by the calibration station. This is particularly valuable since this is the first time on-orbit scale factor determinations have been performed. Along the X-axis, there is a difference of about 5 percent between the average scale factor as determined with data from the calibration station and the data determined from the maneuvers, i.e., 1.01 vs 1.06, respectively. This difference may be partly attributable to knowledge of the location of the Orbiter's center-of-gravity, since a change of only 7.5 cm would account entirely for the difference.

The Y-axis scale factor determined by the calibration station is in excellent agreement with the maneuver data. In this axis there is a slight time dependency (decrease) in the scale factor over the 14 day measurements. The average value over the flight as determined from the calibration stations is slightly higher (about 3 percent) than that obtained from the maneuvers, i.e., 1.14 vs 1.11, respectively. This difference is again

mostly attributable to the lack of knowledge of the location of the Orbiter center-of-gravity.

The Z-axis scale factor as determined by the maneuvers provides more reliable information due to poor quality data in this axis when measured by the calibration station. This was caused by jitter in the driving platform motor. The average scale factor for this axis determined from data from platform motion is 1.14. At present, the more reliable scale factor, 1.075, is that determined during maneuvers.

The combined STS-58 on-orbit bias and scale factors provide the means to achieve an absolute measurement of the residual acceleration on the Orbiter on orbit. This is orders of magnitude superior to past Orbiter pendulous accelerometer systems, such as HiRAP. Specifically, HiRAP bias ground calibrations yield an absolute measurement uncertainty on the order of 80  $\mu\text{g}$  and flight techniques used to improve this uncertainty are on the order of 5  $\mu\text{g}$ ; for OARE, the corresponding uncertainty is about 0.04  $\mu\text{g}$ . This improved performance should directly benefit both national and international on-orbit experimenters.

## References

- <sup>1</sup>Blanchard, R.C., Hendrix, M.K., Fox, J.C., Thomas, D.J., and Nicholson, J.Y., "The Orbital Acceleration Research Experiment," Journal of Spacecraft and Rockets, vol. 24, no. 6, Nov.-Dec. 1987, pp. 504-511.
- <sup>2</sup>ACIP/HiRAP End Item Specification," Drawing No. 3291583, Bendix Corp., Aerospace Systems Div., Ann Arbor, MI, May 1982.
- <sup>3</sup>Blanchard, R.C.; and Rutherford, J.F.: The Shuttle Orbiter High Resolution Accelerometer Package Experiment: Preliminary Flight Results. Journal of Spacecraft and Rockets, vol. 22, no. 4 July-August 1985, p 474.
- <sup>4</sup>Blanchard, R. C., Larman, K. T., and Moats C. D., "Flight Calibration Assessment of HiRAP Accelerometer Data," AIAA Paper 93-0836, January 1993.
- <sup>5</sup>"Microgravity Science and Applications Program Tasks," 1991 revision, NASA TM-4349, February 1992.
- <sup>6</sup>Ott, R. "NASA's Commercial Microgravity Program," AIAA 93-0371, January 1993.
- <sup>7</sup>Wetter, Barry, "Canada's Microgravity Science Program," AIAA 93-0372, January 1993.
- <sup>8</sup>Latorre, R. and Mims, J., "Soviet Approach to Space Manufacturing in Microgravity," AIAA 93-0375, January 1993.
- <sup>9</sup>Rogers, M.J., et al., "Low Gravity Environment On-board Columbia During STS-40," AIAA 93-0833, January 1993.
- <sup>10</sup>Blanchard, R.C., Nicholson, J.Y., and Ritter, J.R., "STS-40 Orbital Acceleration Research Experiment Flight Results During a Typical Sleep Period," Microgravity Science and Technology, vol. 2, 1992, pp. 86-93.
- <sup>11</sup>Blanchard, R.C., Nicholson, J.Y., and Ritter, J.R., "Preliminary OARE Absolute Acceleration Measurements on STS-50," NASA TM-107724, Feb. 1993.
- <sup>12</sup>"Aerodynamic Design Data Book, Vol. 2 Launch Vehicle," release L-7, Rockwell International, April 1982.

<sup>13</sup>McNally, P.J. and Blanchard, R. C., "Comparison of OARE Ground and In-flight Bias Comparisons," AIAA Paper 94-0436, January 1994.

<sup>14</sup>Snadecor, George W. and Cochran, William G., "Statistical Method," 7th ed., Iowa State University Press, 1980, pp. 45-50.

<sup>15</sup>*U.S. Standard Atmosphere, 1976*, NOAA, NASA and U.S. Air Force, Oct. 1976.

<sup>16</sup>"Operational Aerodynamic Design Data Book," Rockwell International, Space Division, Downy, CA STS 85-0118 CHG 3, September 1991.

## APPENDIX

The major low frequency components along the body axes sensed by an accelerometer attached to the Orbiter at a vector distance  $\mathbf{r}$  from the center-of-gravity is given by the following:

$$[\mathbf{A}_{\text{aero}}] + [\mathbf{A}_{\text{gg}} + \mathbf{A}_{\text{oop}}] + [\boldsymbol{\omega} \times (\boldsymbol{\omega} \times \mathbf{r}) + (\dot{\boldsymbol{\omega}} \times \mathbf{r})]$$

1                      2                      3

The details of the models used in this report for each of the quantities enclosed in the brackets above are given in the following sections of this appendix. The numbers under the brackets correspond to the section in which the quantities inside the bracket are discussed.

### 1. Aerodynamics Model

The model for the body axes acceleration vector components ( $\text{m/s}^2$ ) due to aerodynamics is,

$$A_i = \frac{1}{2} \rho V_a^2 \frac{S_{\text{ref}}}{M} C_i \quad (1)$$

where  $i=X_b, Y_b, \text{ or } Z_b$ ,  $\rho$  is the air density ( $\text{kg/m}^3$ ),  $V_a$  is the air relative velocity ( $\text{m/s}$ ),  $S_{\text{ref}}$  is the coefficient reference area ( $249.909\text{m}^2$ ), and  $M$  is the orbiter mass which for this application is 110371.4, 109549.0, and 108935.3 kg (243327.2, 241514.2, and 240161.2 lbs.) for mission elapsed time days 2, 6, and 9 respectively. The density used in the calculations are from the 1976 U.S. Atmosphere Standard.<sup>15</sup>

Coefficient  $C_i$  is related to the body axis aerodynamic coefficients by the following transformation,

$$\begin{aligned} C_x &= -C_A, \\ C_y &= C_Y, \text{ and} \\ C_z &= -C_N \end{aligned} \quad (2)$$

In general, the body axes coefficients are a function of the orientation of the Orbiter with respect to  $V_a$ . Two wind angles are used in the model, namely angle-of-attack,  $\alpha$  and side-slip angle,  $\beta$ . The behavior of the body axes coefficients as a function of these two angles are given in Figs. A1 and A2. These data represent the Orbiter Project Office predictions<sup>16</sup> while on orbit when Orbiter payload doors are open.

## 2. Gravity induced accelerations

In general, if the OARE sensor is located anywhere in the Orbiter other than its center-of-gravity, the Earth's gravitational field will induce a small acceleration in the sensor. If the sensor is above or below the center-of-gravity, an acceleration will result from the gradient of the gravitational field, i.e., a gravity gradient effect. If the sensor is not in line with the vector from the Earth's center to the Orbiter's center-of-gravity, an acceleration is induced in the sensor in the horizontal plane toward the orbiter center-of-gravity. In this report, this component of induced acceleration is referred to as an "out-of-plane" effect.

### i. VERTICAL DIRECTION (GRAVITY-GRADIENT)

If  $\mathbf{r}_s$  is the vector in space from the Orbiter's center of gravity to the OARE sensor location,  $X_s$ ,  $Y_s$ , and  $Z_s$  are its components along the respective Orbiter body axes. That is,

$$\mathbf{r}_s = X_s \hat{\mathbf{x}}_b + Y_s \hat{\mathbf{y}}_b + Z_s \hat{\mathbf{z}}_b \quad ,$$

where  $\hat{\mathbf{x}}_b$ ,  $\hat{\mathbf{y}}_b$ , and  $\hat{\mathbf{z}}_b$  are unit vectors giving the body axes orientations.

The unit vector corresponding to the position vector of the Orbiter center of gravity from the Earth's center is,

$$\hat{\mathbf{r}} \equiv \frac{\mathbf{r}}{r}$$

The difference in vertical height between the Orbiter center of gravity and the OARE sensor is calculated from,

$$\Delta h = \mathbf{r}_s \cdot \hat{\mathbf{r}}$$

That is,

$$\Delta h = X_s \cos \theta_a + Y_s \cos \theta_b + Z_s \cos \theta_c$$

where  $\theta_a$  is the angle between the Orbiter X-axis and the radius vector (Earth center to Orbiter),  $\theta_b$  the Orbiter Y-axis, and  $\theta_c$  the Orbiter Z axis. Thus, the acceleration at the OARE sensor location along the radius vector is then found by,

$$A_r = - k_r \Delta h,$$

where  $k_r$  is the induced acceleration per unit distance from the center of gravity. The negative sign is due to the fact that a force up is interpreted by the sensor as an acceleration downward and vice versa.

The accelerations sensed in the OARE x, y, and z sensor axes is then found by,

$$A_x = -k_\tau \Delta h \cos \phi_a$$

$$A_y = -k_\tau \Delta h \cos \phi_b$$

$$A_z = -k_\tau \Delta h \cos \phi_c$$

where  $\phi_a$  is the angle between the OARE sensor X-axis and the radius vector,  $\phi_b$  the OARE sensor y-axis, and  $\phi_c$  the OARE sensor z-axis.

Assuming an altitude of 320 km, a 1.0 m displacement (up or down) results in an acceleration change of approximately  $2.663 \times 10^{-6} \text{ m/s}^2$ , or

$$k_\tau = 0.2715 \text{ } \mu\text{g/m} .$$

Changes in altitude of 10 km represent a change in  $k_\tau$  of 1.2 ng/m.

## ii. HORIZONTAL DIRECTION (OUT-OF-PLANE)

This induced acceleration is caused by the horizontal displacement of the OARE sensor from the Orbiter center of gravity.

As defined earlier,  $\mathbf{r}_s$  represents the vector from the Orbiter center-of-gravity to the OARE sensor in space and  $\hat{\mathbf{r}}$  is a unit vector from the Earth's center to the Orbiter center of gravity. Then,

$$\mathbf{r}_h = (\hat{\mathbf{r}} \times \mathbf{r}_s) \times \hat{\mathbf{r}} ,$$

where  $\mathbf{r}_h$  is a vector representing the component of  $\mathbf{r}_s$  in the horizontal plane. The acceleration along this vector is,

$$\mathbf{A}_h = k'_\tau \mathbf{r}_h ,$$

where  $k'_\tau = \frac{1}{2} k_\tau$ , so that at 320 km,  $k'_\tau = 0.1358 \text{ } \mu\text{g}$ .

The acceleration induced in each of the OARE sensor's axes are equal to the components of  $\mathbf{A}_h$ , that is,

$$A_x = k'_\tau \mathbf{A}_h \cdot \hat{\mathbf{x}}_s$$

$$A_y = k'_\tau \mathbf{A}_h \cdot \hat{\mathbf{y}}_s$$

$$A_z = k'_\tau \mathbf{A}_h \cdot \hat{\mathbf{z}}_s$$

where  $\hat{\mathbf{x}}_s$ ,  $\hat{\mathbf{y}}_s$ , and  $\hat{\mathbf{z}}_s$  are unit vectors corresponding to the OARE sensor axes orientation in space.

### 3. Rotation induced acceleration

Let  $\omega$  be the angular rotation vector of the Shuttle about its center-of-gravity,  $\omega_s$  be the angular rotation vector of the calibration table with respect to the Shuttle,  $r$  be the vector from the Shuttle center-of-gravity to the sensor, and  $R_s$  be the vector from the calibration table center of rotation to the sensor. The rotation induced acceleration in the sensor will have the following terms:

$$\begin{aligned} & \dot{\omega} \times r + \dot{\omega}_s \times R_s \text{ (tangential acceleration terms)} \\ & + \omega \times (\omega \times r) + \omega_s \times (\omega_s \times R_s) \text{ (centripetal acceleration terms)} \\ & + 2 \omega \times (\omega_s \times R_s) \text{ (Coriolis acceleration term)} \end{aligned}$$

If the Shuttle is rotating, but the calibration table is fixed relative to the Shuttle (i.e.,  $\omega_s = 0$ ), the the remaining terms are:

$$\dot{\omega} \times r + \omega \times (\omega \times r)$$

This expression can be written in components along the body axes. Let  $X_s, Y_s, Z_s$  represent the distances along the respective Orbiter body axes from the Orbiter center of gravity to the OARE sensor location; let  $p, q,$  and  $r$  be the rotation rates (angular velocities) in rad/s about the Orbiter's  $x, y,$  and  $z$  body axes; and  $\dot{p}, \dot{q},$  and  $\dot{r}$  be the corresponding angular accelerations. Then,

$$\begin{pmatrix} A_{x_b} \\ A_{y_b} \\ A_{z_b} \end{pmatrix} = K_0 \begin{pmatrix} -(q^2 + r^2) & pq - \dot{r} & pr + \dot{q} \\ pq + \dot{r} & -(p^2 + r^2) & qr - \dot{p} \\ pr - \dot{q} & qr + \dot{p} & -(p^2 + q^2) \end{pmatrix} \begin{pmatrix} X_s \\ Y_s \\ Z_s \end{pmatrix}$$

where  $A_{x_b}, A_{y_b},$  and  $A_{z_b}$  are rotation-induced accelerations (in  $\mu g$ 's) in the Orbiter's  $X_b, Y_b,$  and  $Z_b$  axes.  $K_0 = 1.02 \times 10^5$  converts accelerations from  $m/s^2$  to  $\mu g$ 's when  $r$  is in meters.

In most cases, the contributions due to  $\dot{p}, \dot{q},$  and  $\dot{r}$  can be neglected. However, in the case of maneuvers, during which rotation rates approach 1.0 deg/s, they are considered. The contributions due to  $\dot{p}, \dot{q},$  and  $\dot{r}$  can also be significant when coupling exists between  $p, q,$  and  $r$ .

Lastly, the rotation induced accelerations along the Orbiter body axes are converted to accelerations in the OARE sensor axes ( $A_x$ ,  $A_y$ ,  $A_z$ ) by a matrix  $[T]$ . This matrix contains the components of each Orbiter body axis along each sensor axis. That is,

$$\begin{pmatrix} A_x \\ A_y \\ A_z \end{pmatrix} = T \begin{pmatrix} A_{x_b} \\ A_{y_b} \\ A_{z_b} \end{pmatrix}$$

where,

$$T = \begin{pmatrix} 1 & 0 & 0 \\ 0 & 0 & -1 \\ 0 & 1 & 0 \end{pmatrix}$$

This represents the only orientation of the calibration platform which was used during maneuvers on STS-58. The very small misalignments between the orbiter body axes and the OARE axes have been neglected for the purpose of this report.



**Table 2 Results from OARE Flight Maneuvers on STS-58**

**(i) SCALE FACTORS**

Maneuver No.	MET Day	Body Axis	Pitch	Maneuver Yaw	Roll
1	2	X	1.07	1.07	*
		Y	*	1.07	0.66
		Z	1.10	*	1.10
2 <sup>†</sup>	6	X	1.07	1.06	*
		Y	*	1.07	1.00
		Z	1.11	*	1.12
3	9	X	1.06	1.05	*
		Y	*	1.08	0.77
		Z	1.11	*	1.11

† Aborted during roll maneuver

**(ii) AVERAGE INDUCED ACCELERATION (ug)**

Maneuver No.	MET Day	Body Axis	Pitch	Maneuver Yaw	Roll
1	2	X	67.0	38.6	*
		Y	*	-4.2 <sup>††</sup>	0.59
		Z	-57.5	*	-42.4
2	6	X	71.6	40.0	*
		Y	*	-5.0 <sup>††</sup>	0.56
		Z	-61.4	*	-44.2
3	9	X	72.1	39.8	*
		Y	*	-4.0 <sup>††</sup>	.74
		Z	-61.4	*	-36.9

†† Large mid-maneuver altitude correction

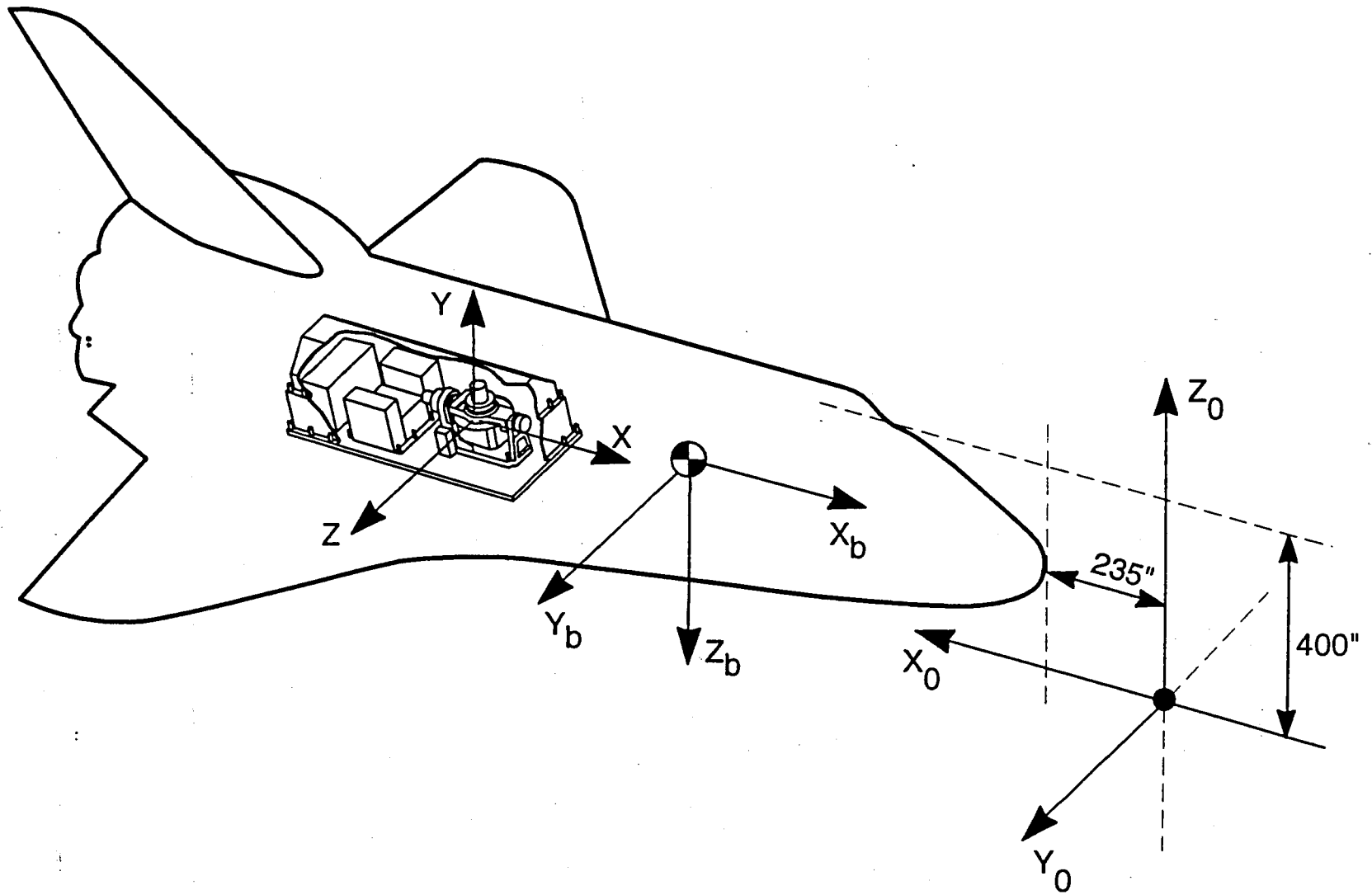


Fig. 1 OARE (X, Y, Z), body axes ( $X_b, Y_b, Z_b$ ), and Orbiter reference ( $X_0, Y_0, Z_0$ ) coordinate systems.

Interface electronics  
(eg. time code, tape recorder, GSE)

Computer  
• 16 bit processor  
• Programmable  
• 4 MByte memory

GSE port

Servo control  
of cal table

Power system

Sensor package  
• 3 axis (non-pendulous)  
• 3 ranges ( $10^4$ ,  $10^3$ ,  $10^2$ ,  $\mu\text{g}$ )

WT: 117 lbs  
Size: 17"x13"x41"  
Power: 110 watts

Fig. 2. OARE packing layout sketch.

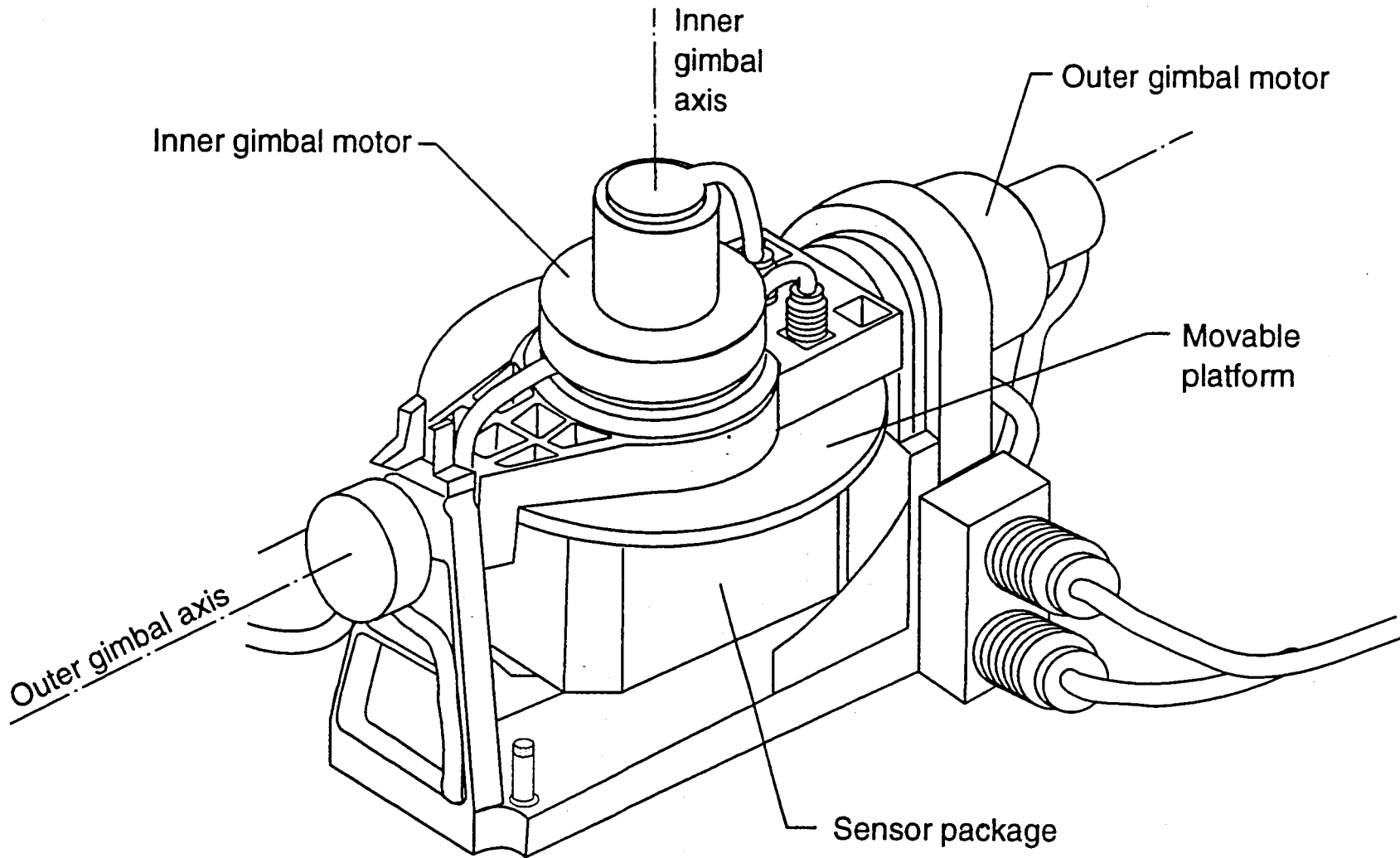
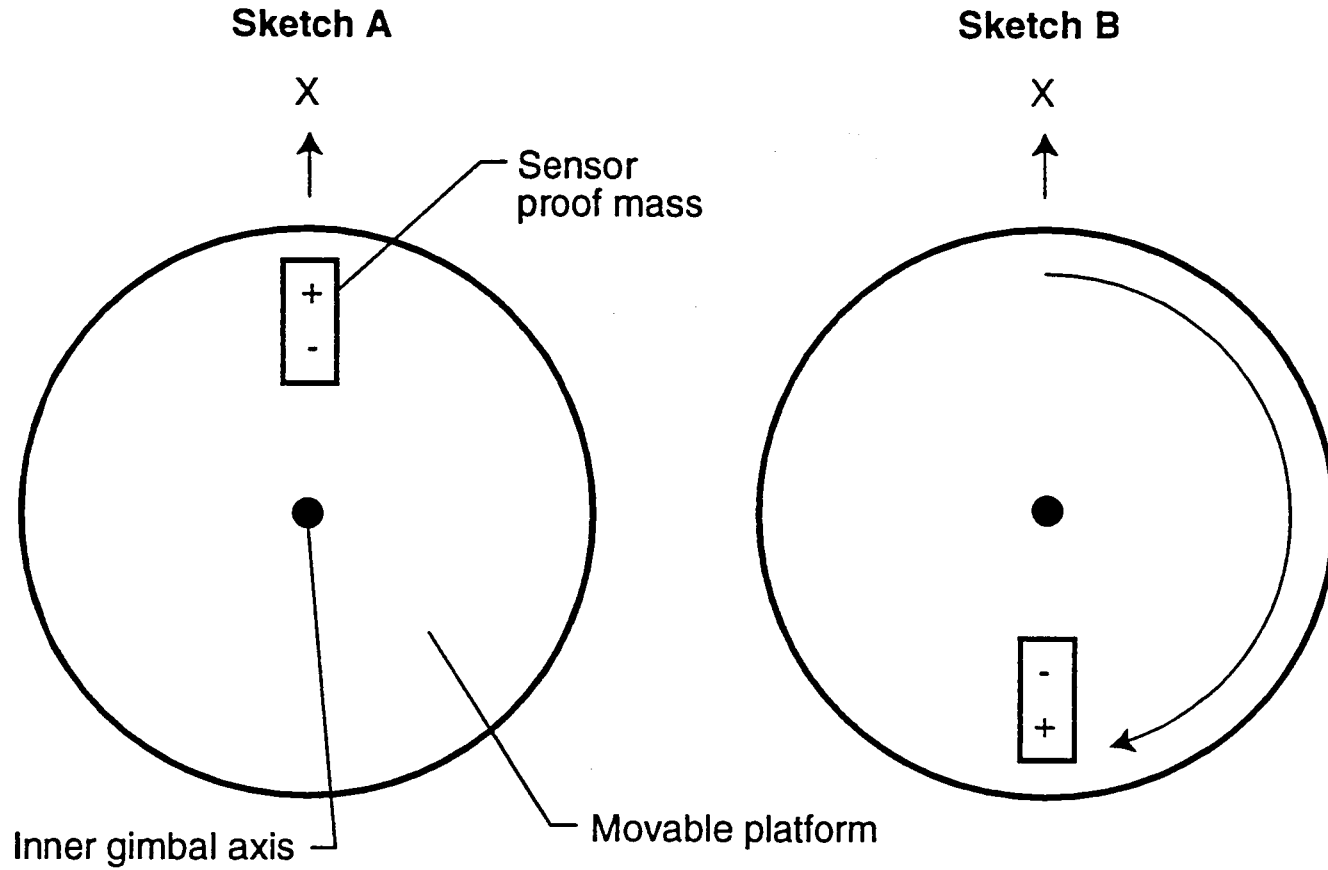


Fig. 3. Calibration table assembly.



**Table at 0 degrees**

$$A_{X_0} = S_X + B_X$$

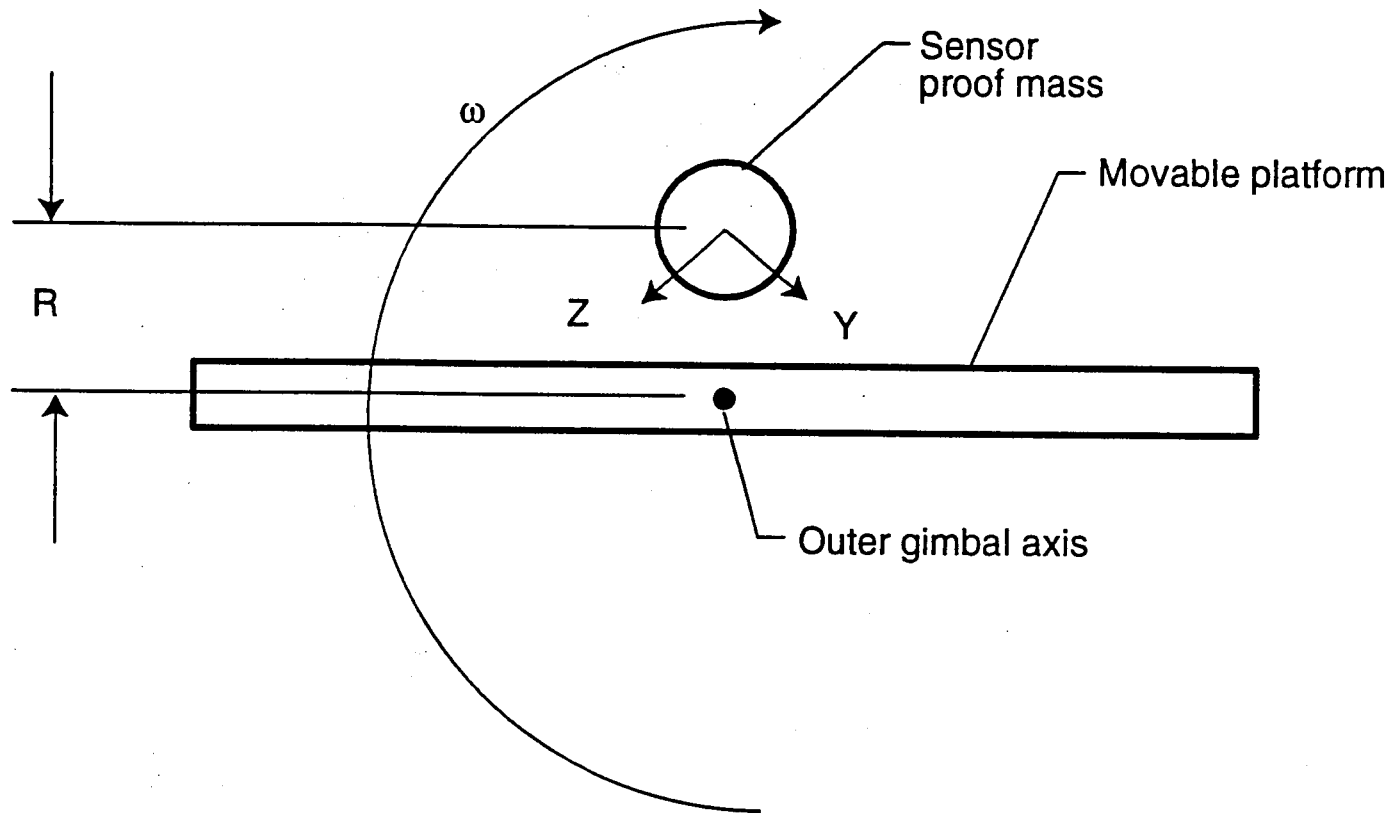
**Table at 180 degrees**

$$A_{X_{180}} = -S_X + B_X$$

$$\text{Add: } A_{X_0} + A_{X_{180}} = 2B_X$$

$$\text{Subtract: } A_{X_0} - A_{X_{180}} = 2S_X$$

Fig. 4. X-axis bias calibration illustration.



$$\text{Scale factor} = \frac{\omega^2 R}{A_s}$$

Fig. 5. Scale factor calibration illustration.

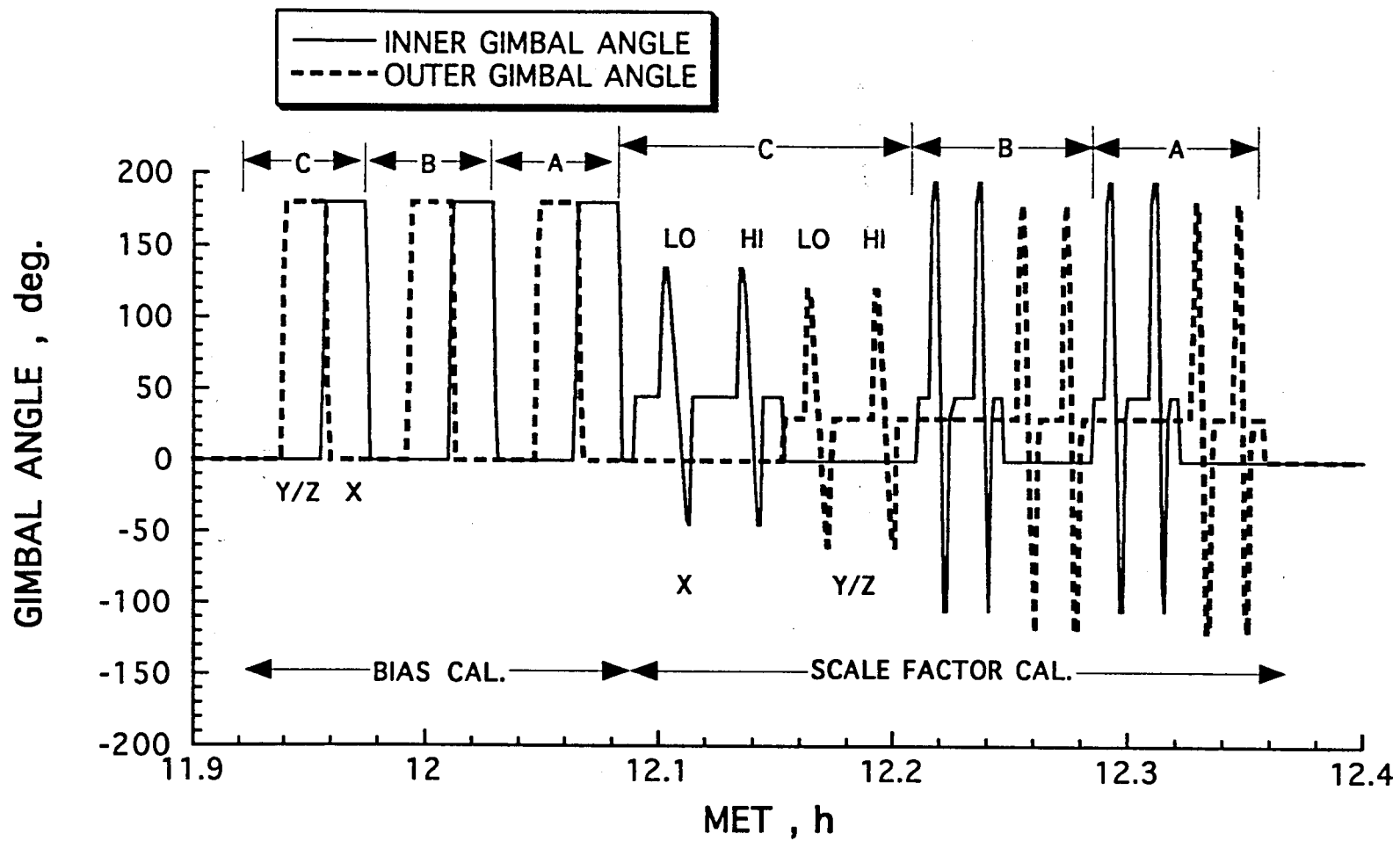


Fig. 6 Typical inner and outer gimbal angle measurements during a calibration sequence.

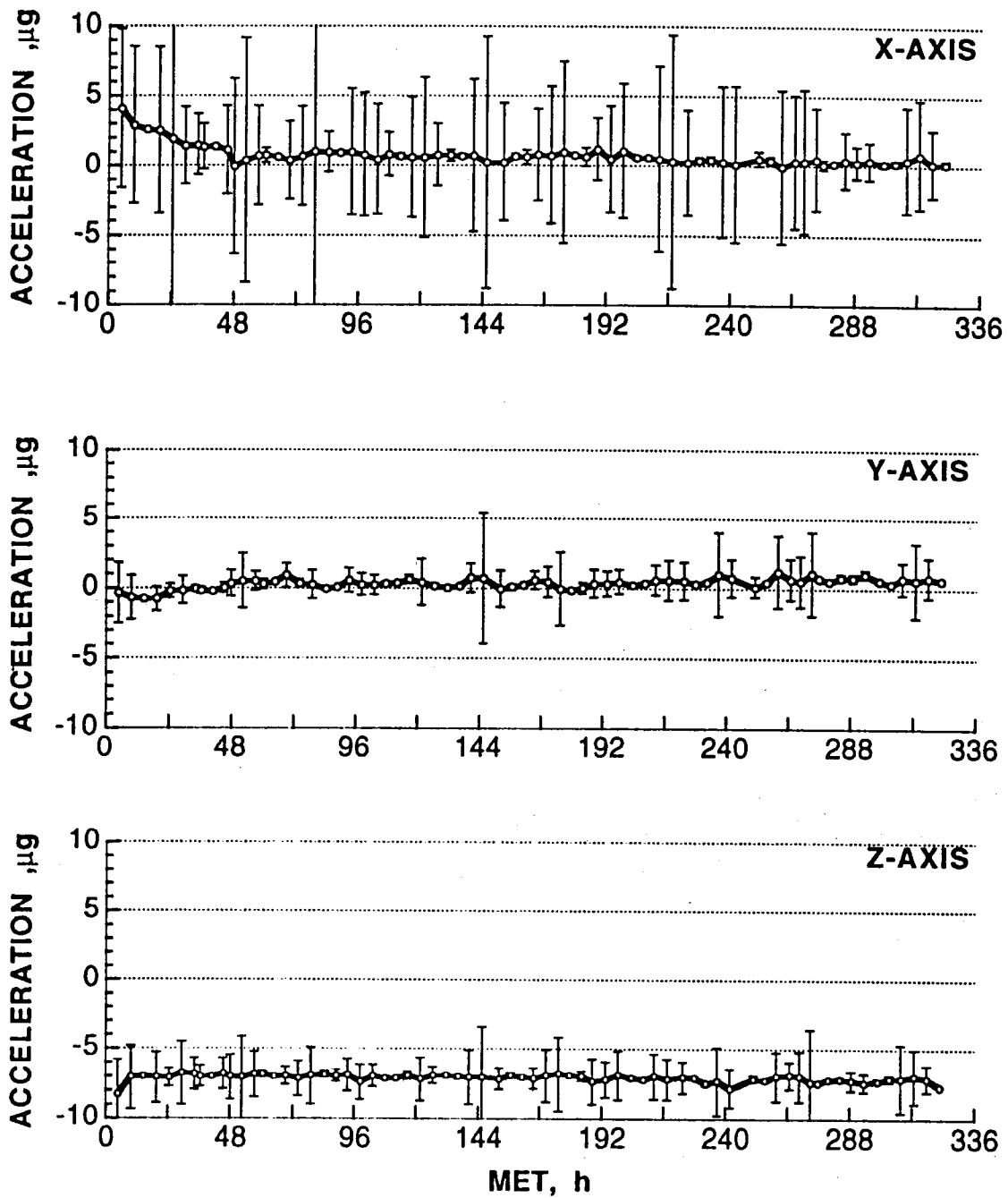


Fig. 7 OARE STS-58 bias measurements with average deviations.

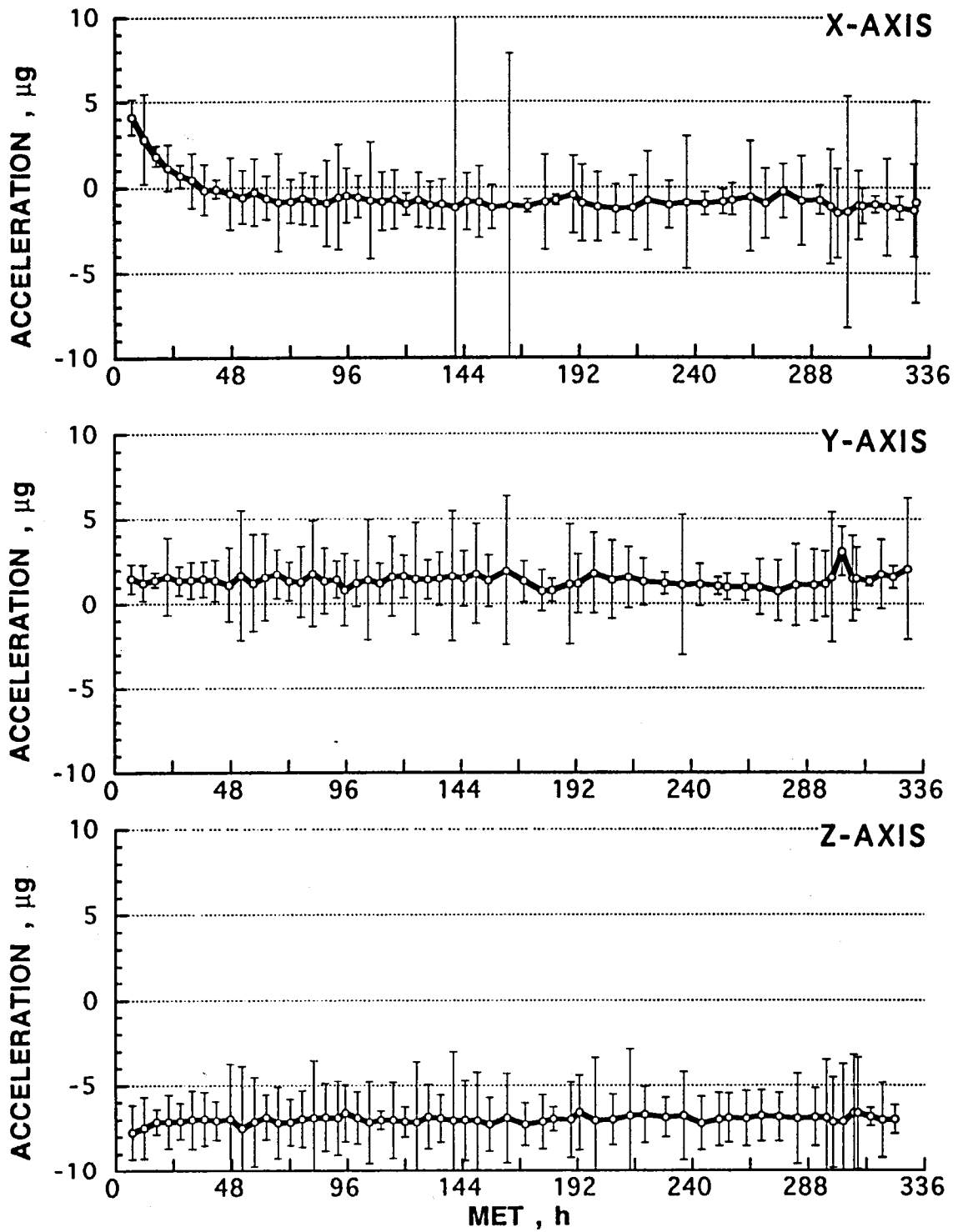


Fig. 8 OARE STS-50 bias measurements with average deviations.

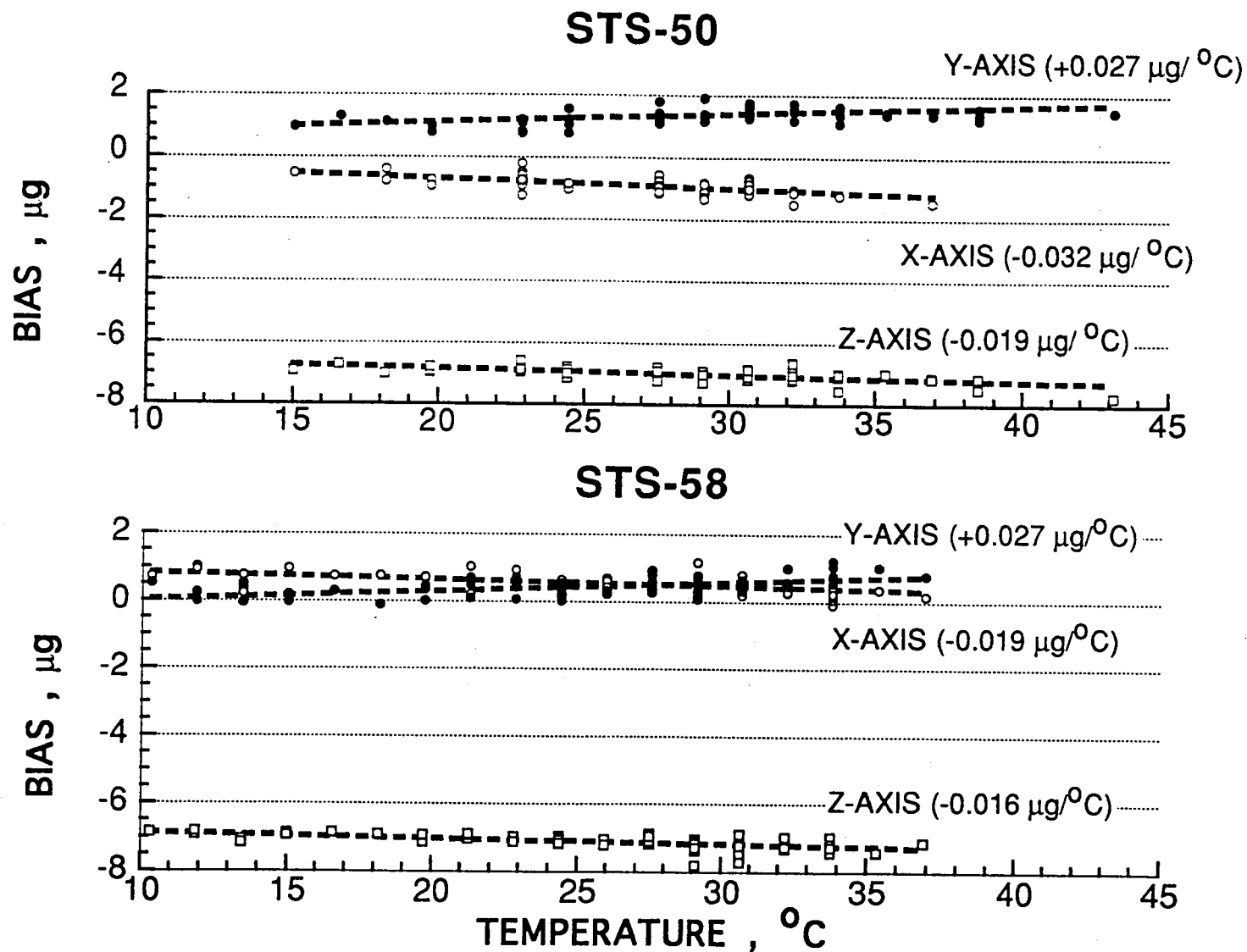


Fig. 9 Comparison of OARE STS-58 in-flight bias temperature sensitivity measurements with corresponding STS-58 measurements

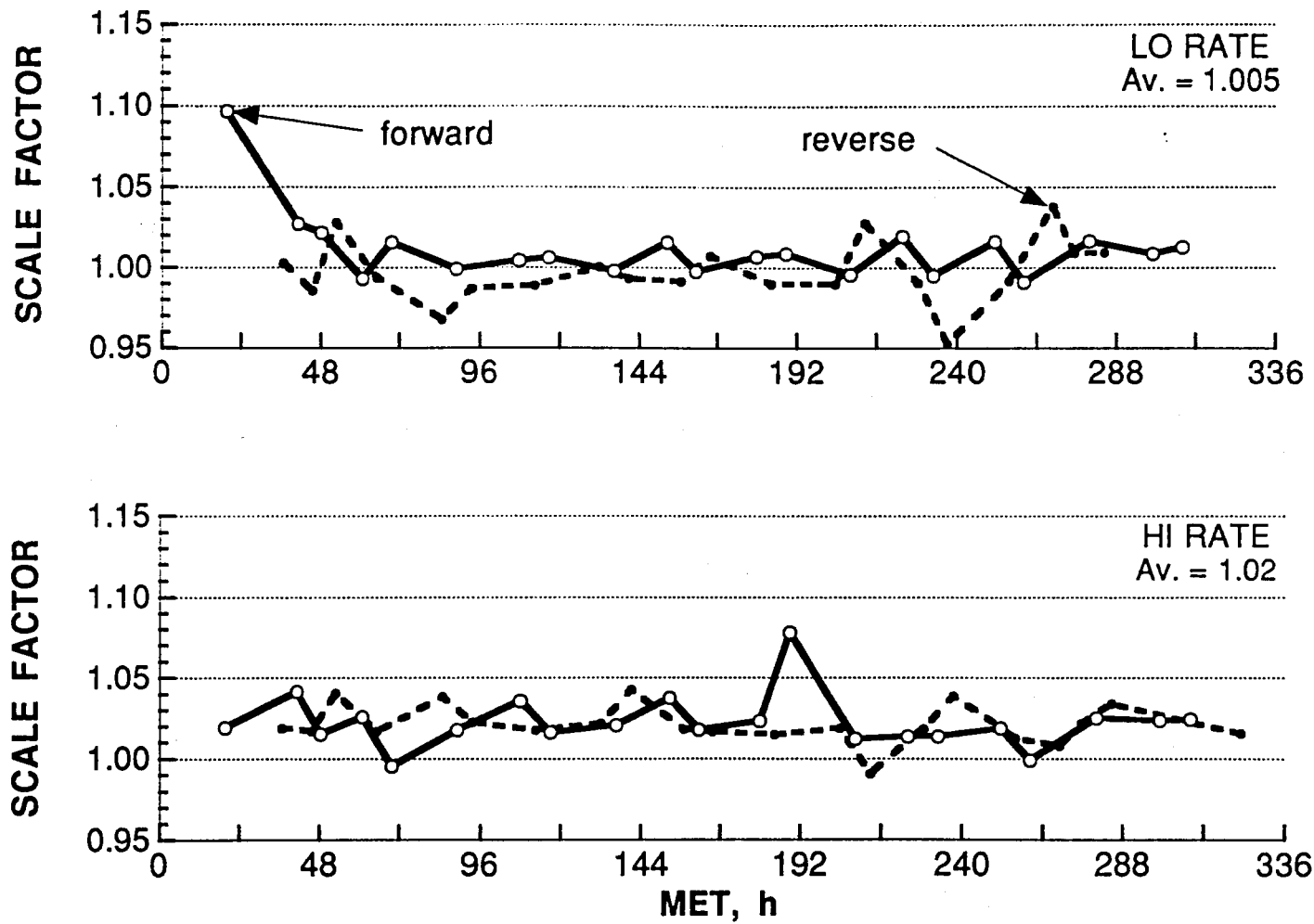


Fig. 10 OARE X-axis, C-range, scale factor measurements on STS-58

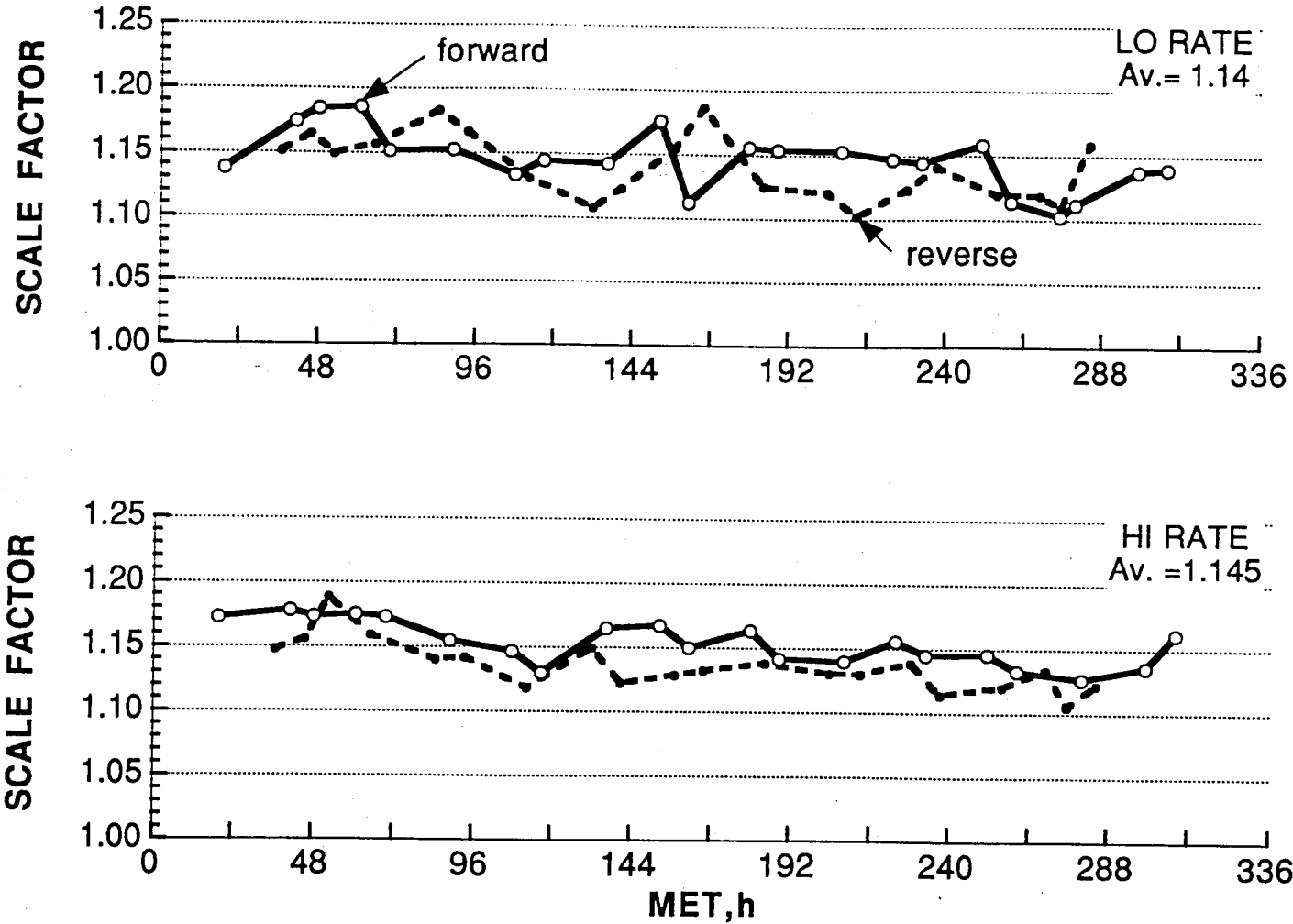


Fig. 11 OARE Y-axis, C-range, scale factor measurements on STS-58

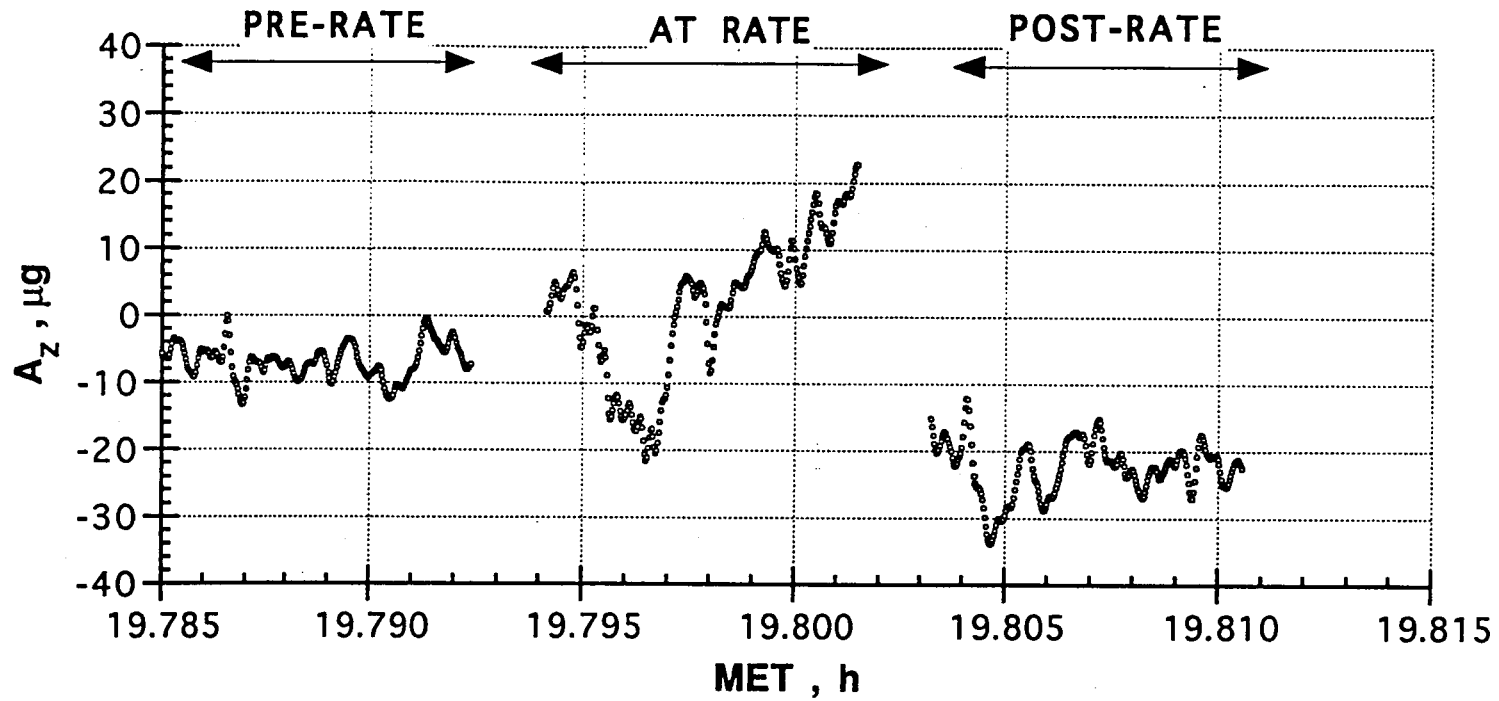


Fig. 12 Typical Z-axis scale factor data, forward direction, low rate.

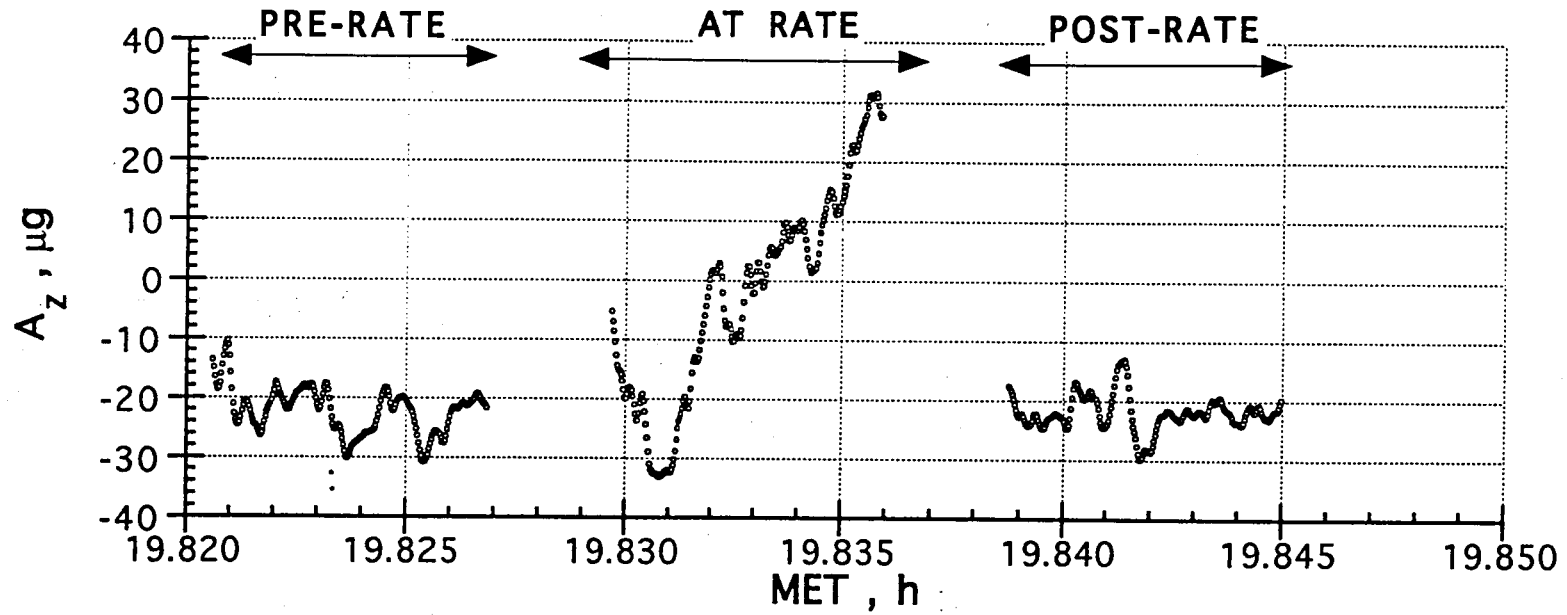


Fig. 13 Typical Z-axis scale factor data, forward direction, high rate

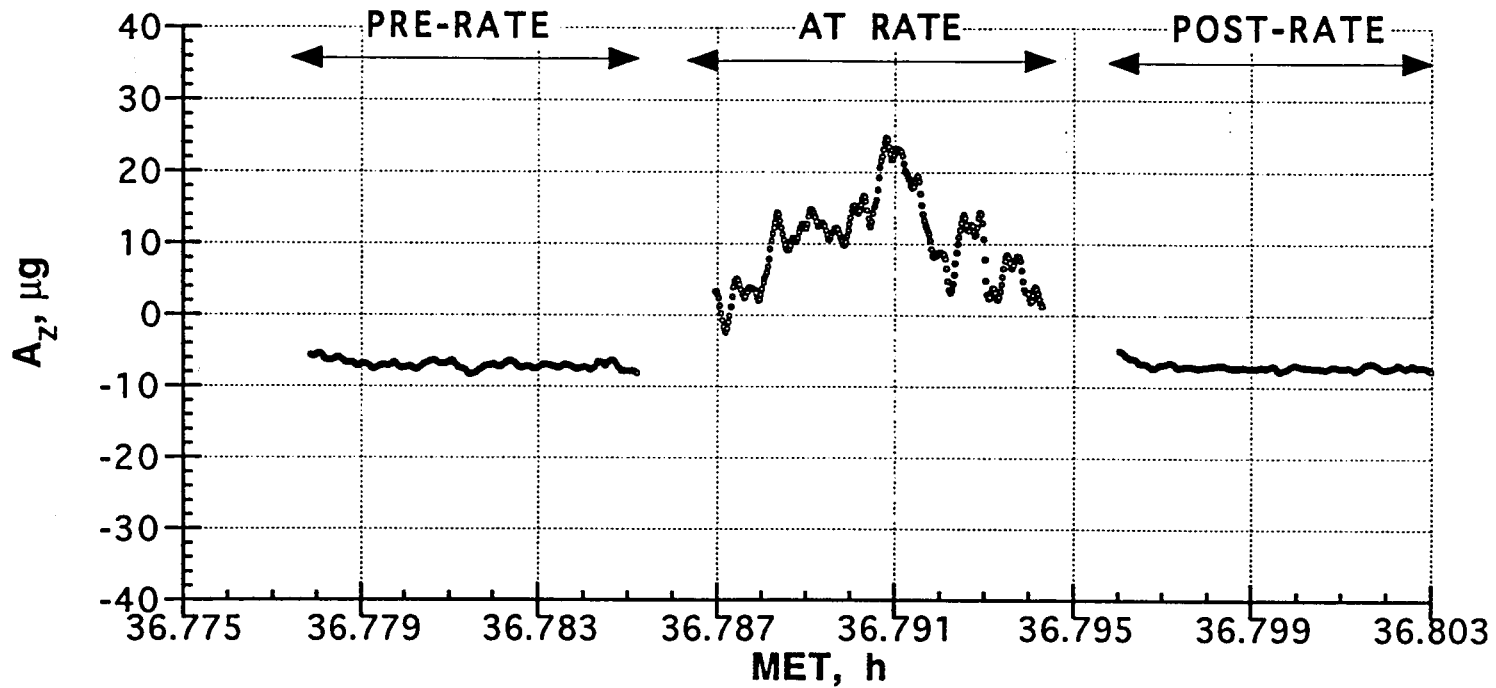


Fig. 14 Typical Z-axis scale factor data, reverse direction, low rate

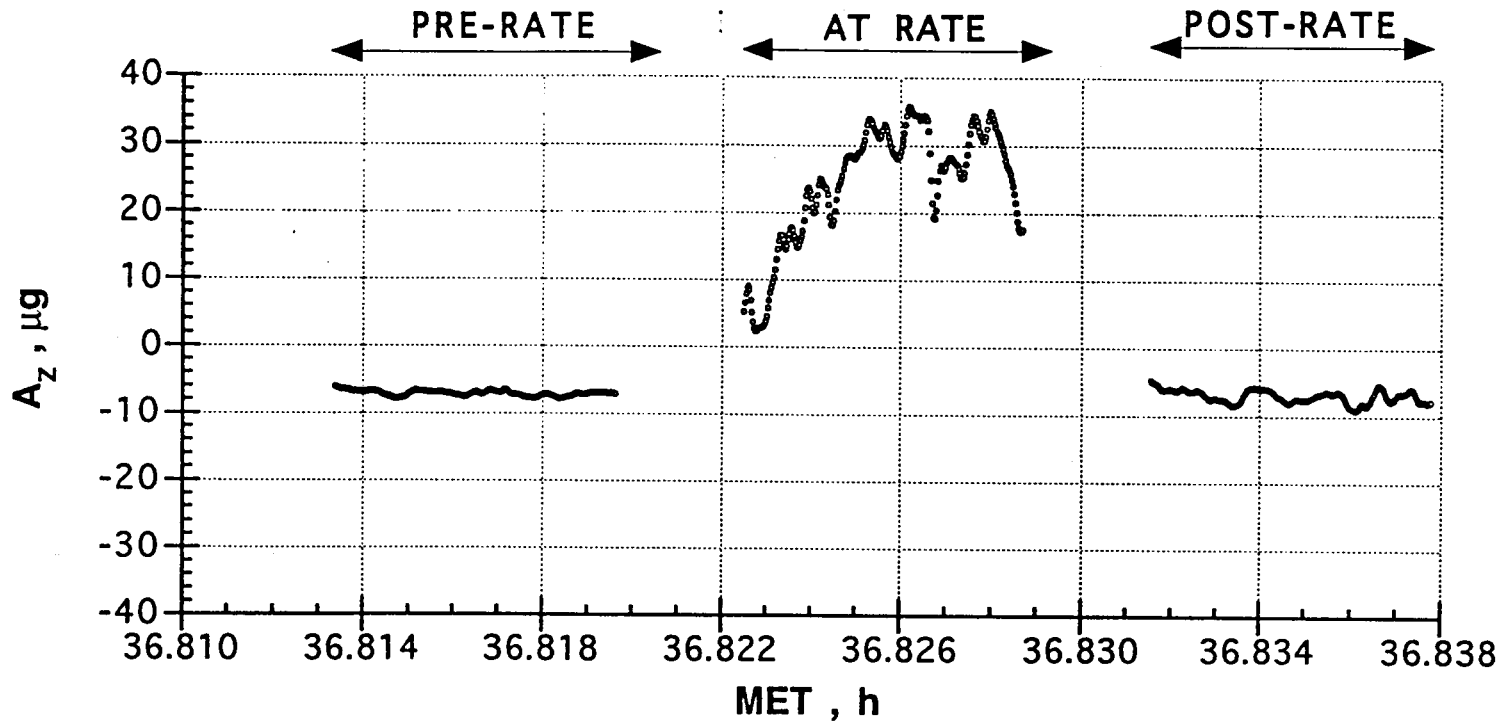


Fig. 15 Typical Z-axis scale factor data, reverse direction, high rate

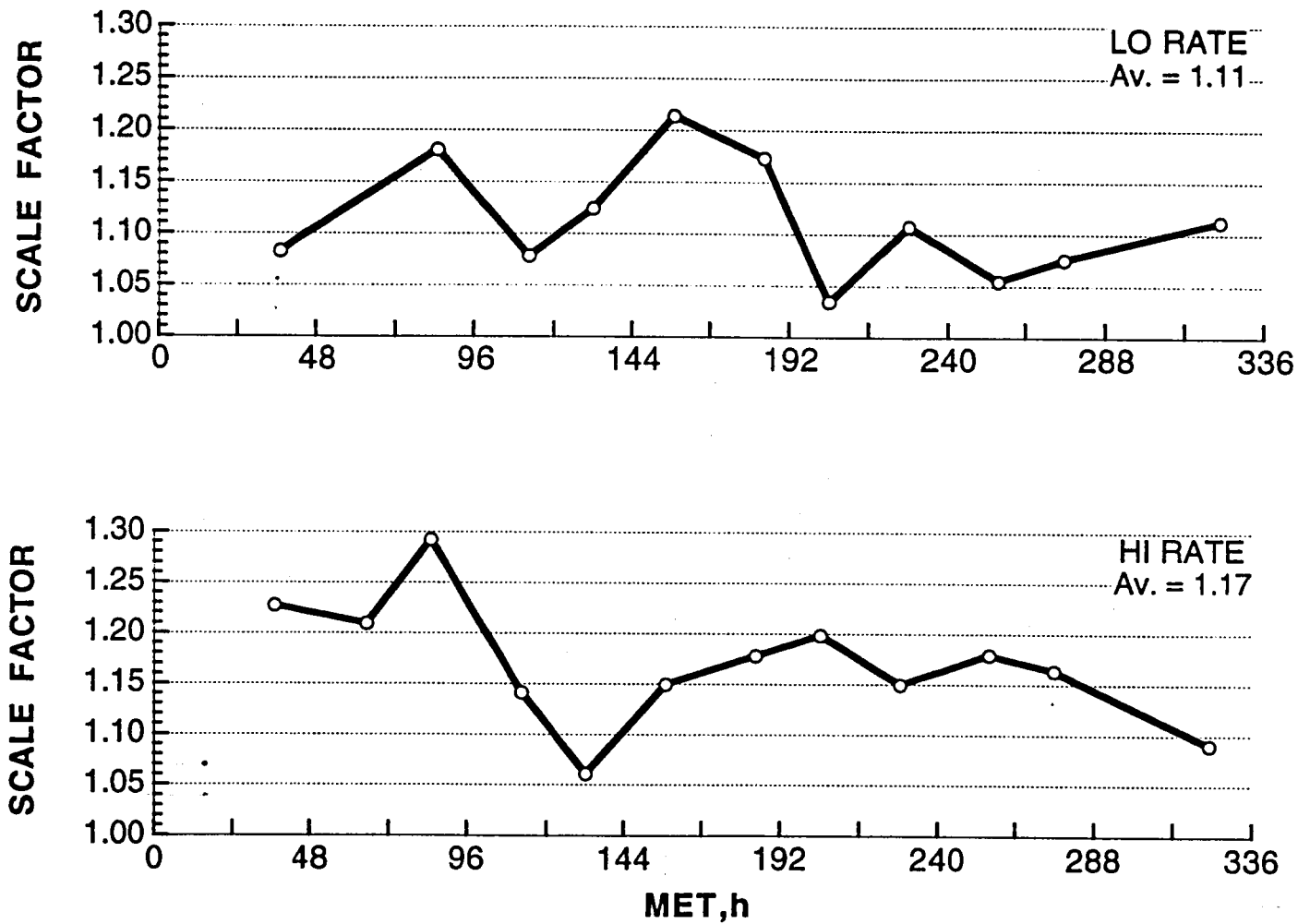


Fig. 16 Z-axis scale factor measurements on STS-58

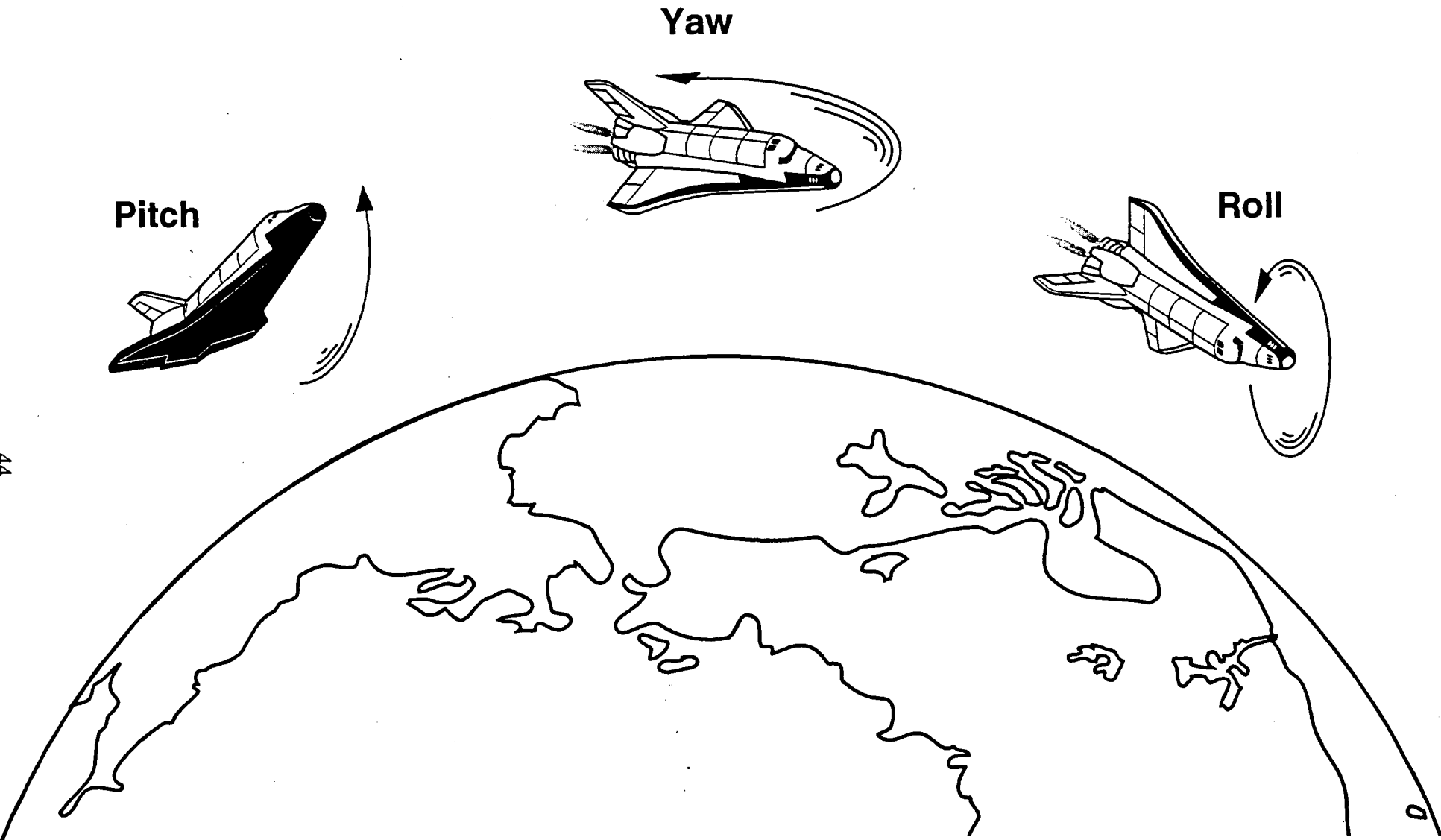


Fig. 17 OARE flight maneuvers.

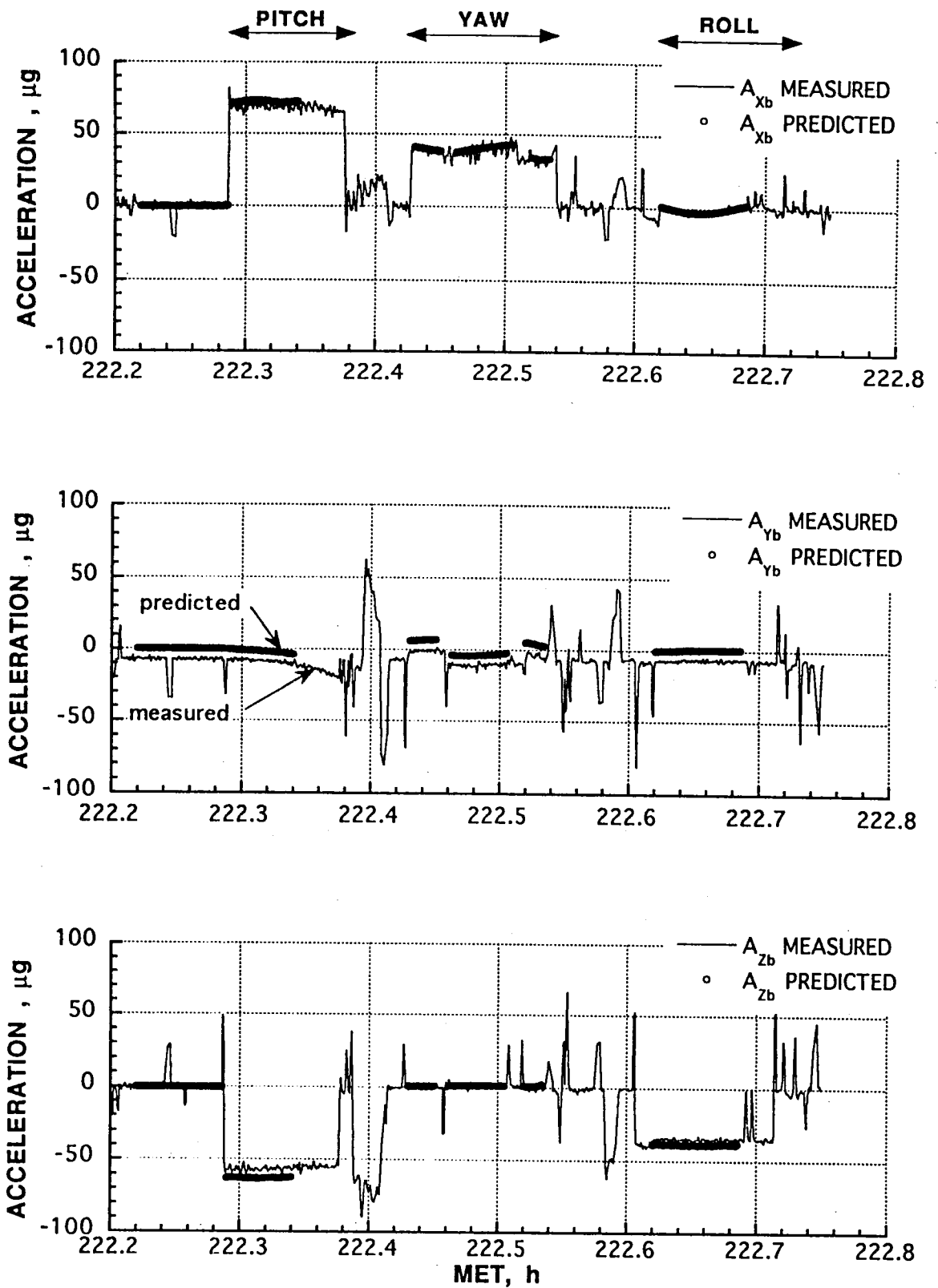


Fig. 18 Comparison of OARE measurements (nominal scale factor and no bias adjustment) with predicted acceleration during maneuver #3.

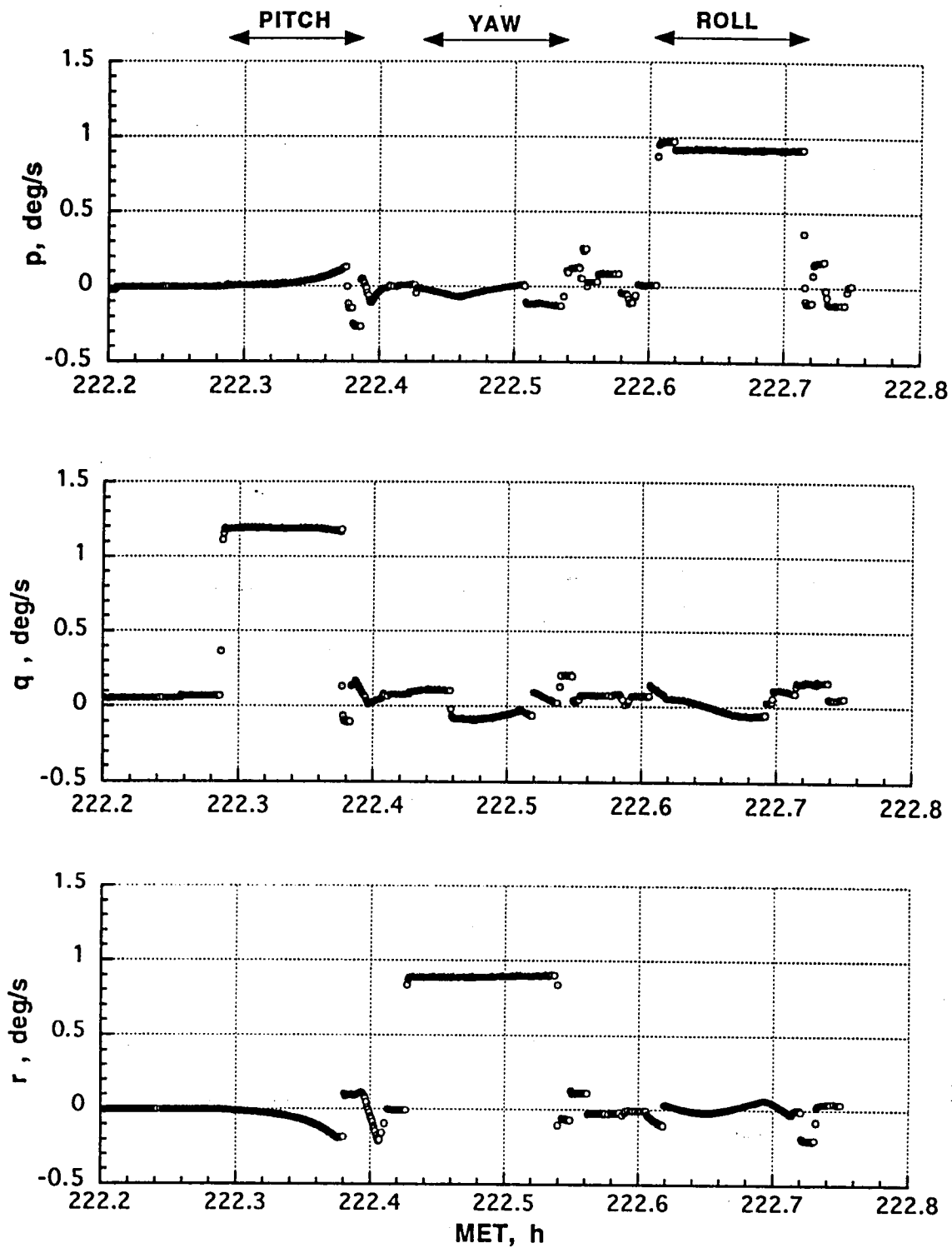


Fig. 19 Body rates during maneuver #3.

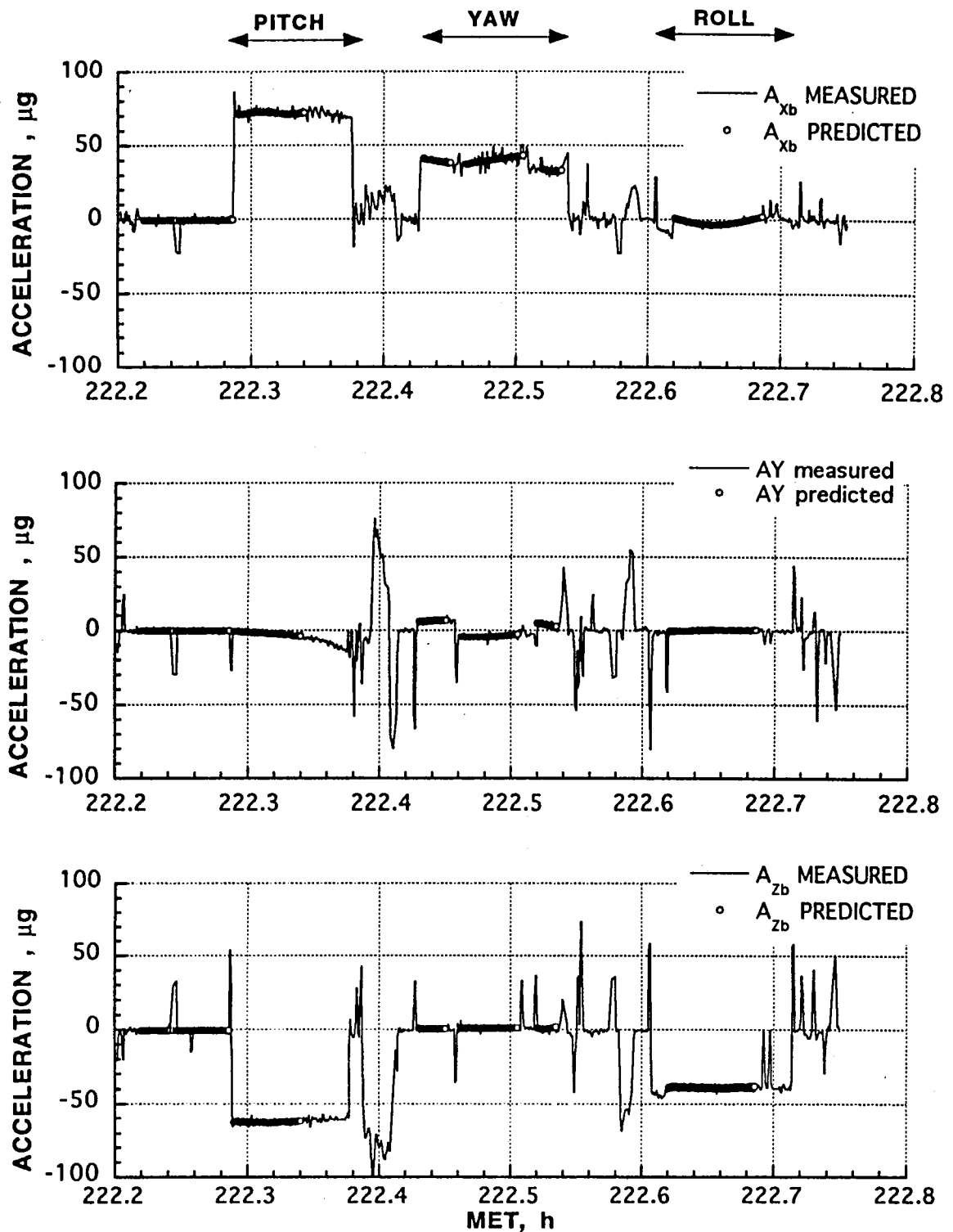


Fig. 20 Comparison of OARE measurements (after scale factor and bias adjustments) with predicted accelerations during maneuver #3.

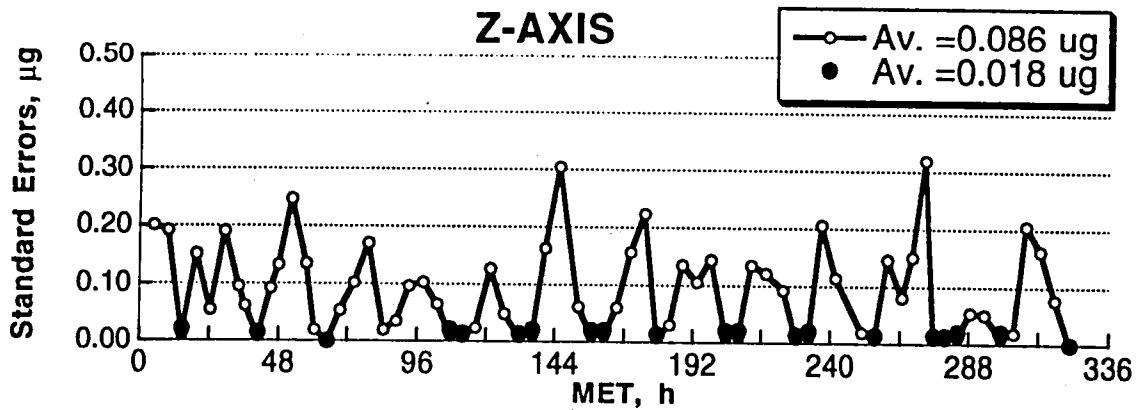
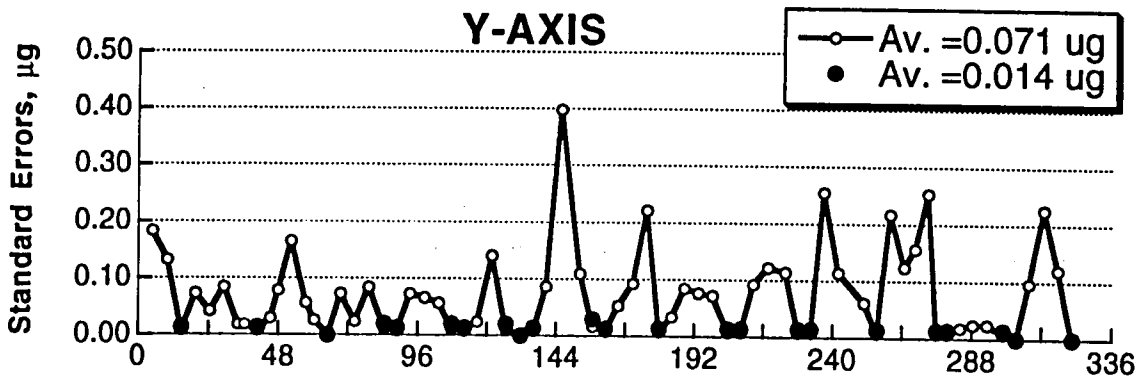
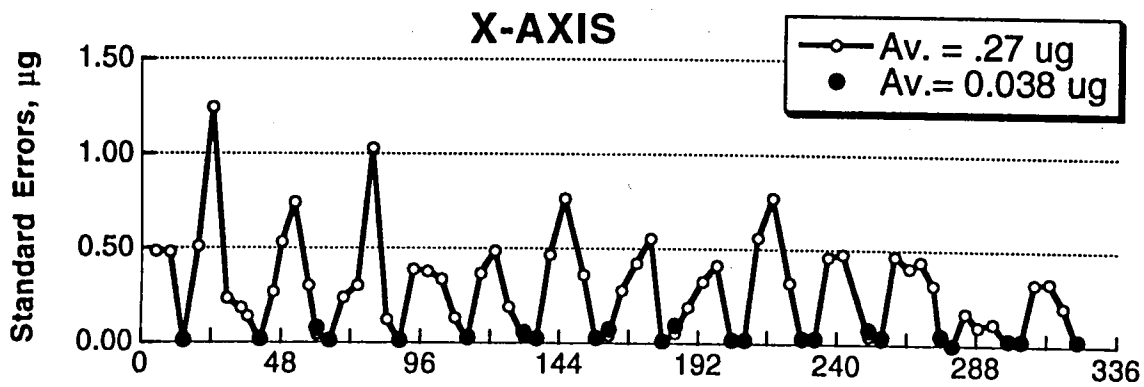


Fig. 21 In-flight bias measurements average standard errors during STS-58

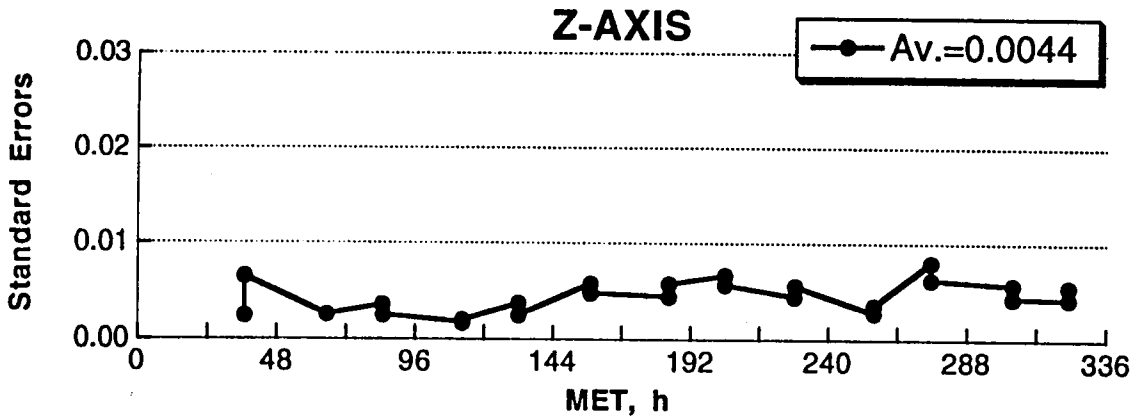
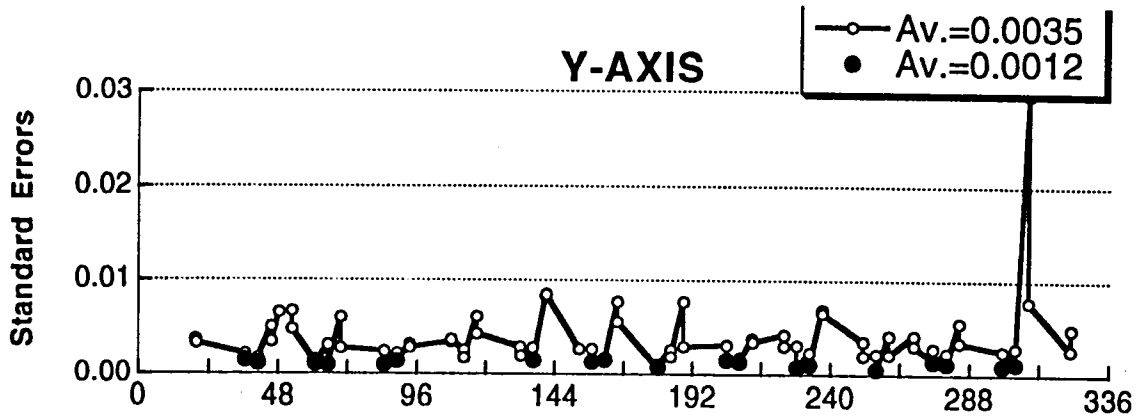
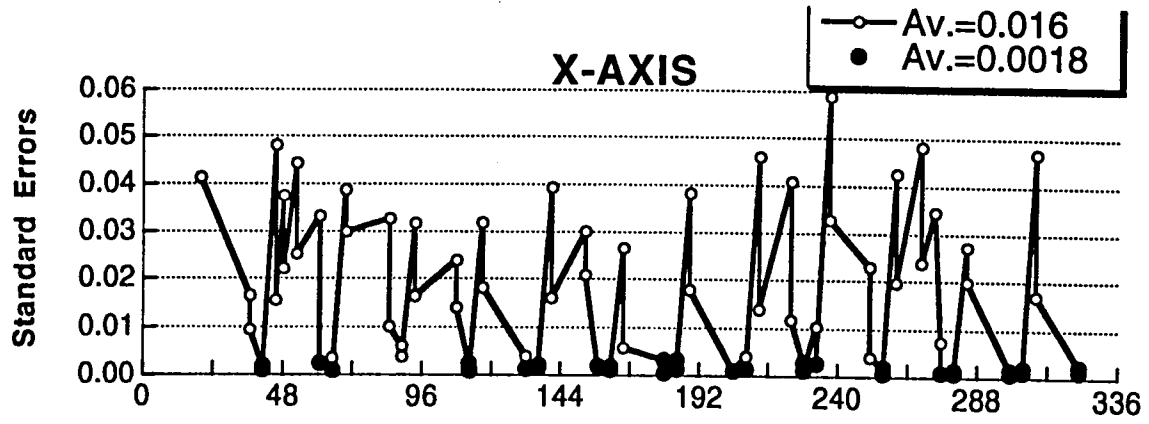


Fig. 22 STS-58 in-flight scale factor measurement average standard errors.

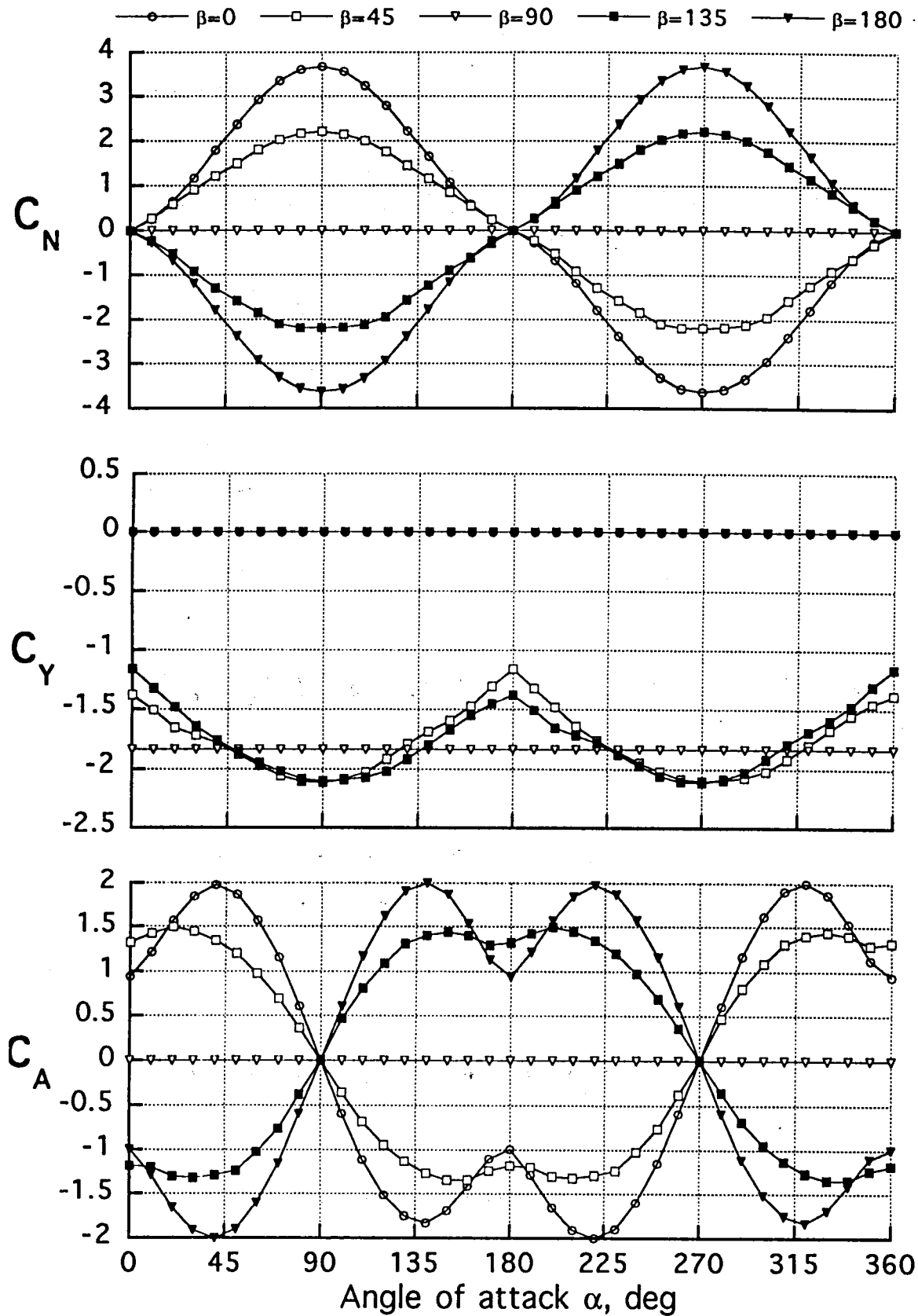


Fig. A1 Free molecule flow force coefficients for selected sideslip angles (payload bay doors open)

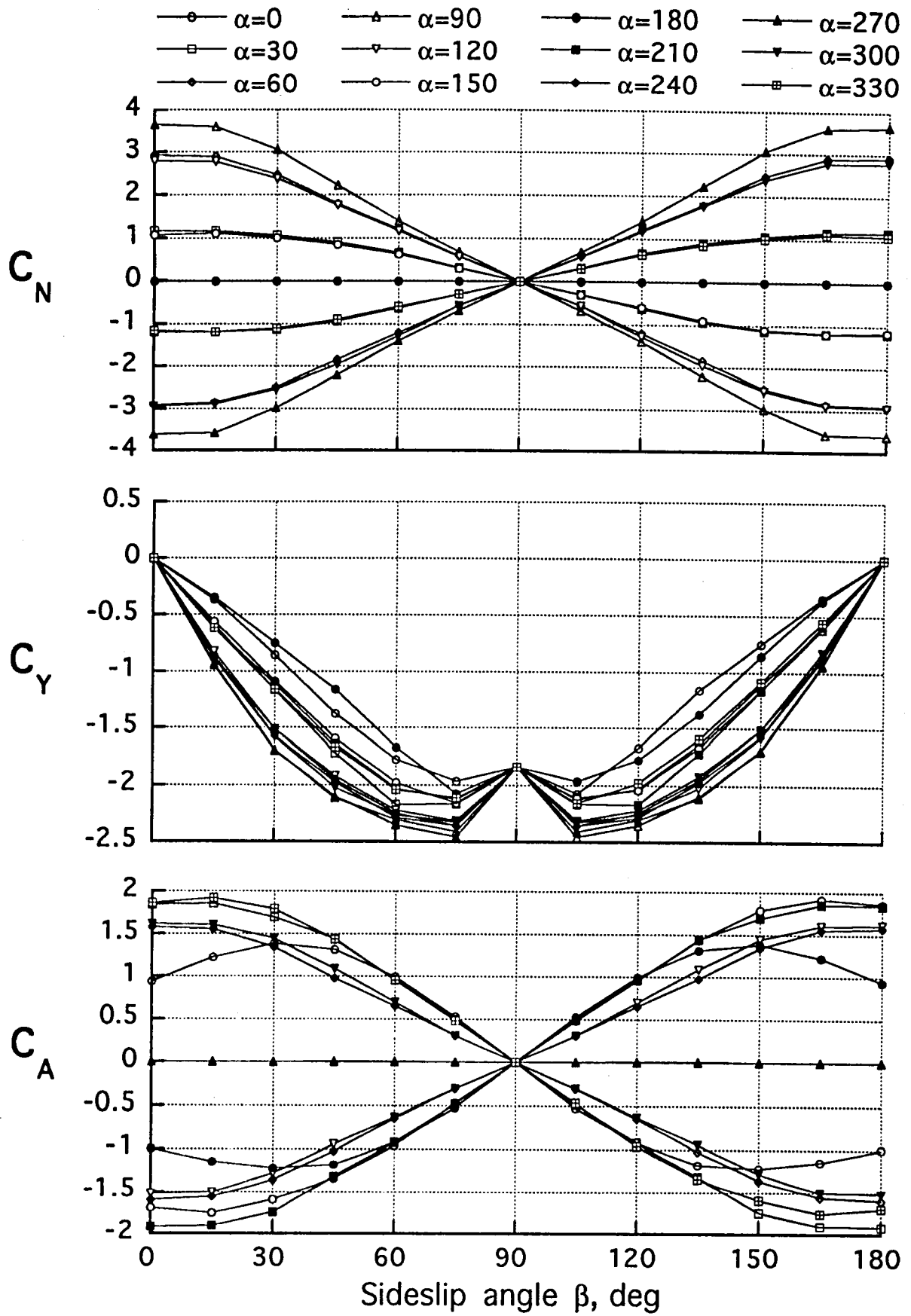


Fig. A2 Free molecule flow force coefficients for selected angles of attack (payload bay doors open)

# REPORT DOCUMENTATION PAGE

*Form Approved*  
OMB No. 0704-0188

Public reporting burden for this collection of information is estimated to average 1 hour per response, including the time for reviewing instructions, searching existing data sources, gathering and maintaining the data needed, and completing and reviewing the collection of information. Send comments regarding this burden estimate or any other aspect of this collection of information, including suggestions for reducing this burden, to Washington Headquarters Services, Directorate for Information Operations and Reports, 1215 Jefferson Davis Highway, Suite 1204, Arlington, VA 22202-4302, and to the Office of Management and Budget, Paperwork Reduction Project (0704-0188), Washington, DC 20503.

<b>1. AGENCY USE ONLY (Leave blank)</b>		<b>2. REPORT DATE</b> April 1994	<b>3. REPORT TYPE AND DATES COVERED</b> Technical Memorandum	
<b>4. TITLE AND SUBTITLE</b> OARE Flight Maneuvers and Calibration Measurements on STS-58			<b>5. FUNDING NUMBERS</b> WU 237-02-02-11	
<b>6. AUTHOR(S)</b> Robert C. Blanchard, John Y. Nicholson, James R. Ritter, and Kevin T. Larman				
<b>7. PERFORMING ORGANIZATION NAME(S) AND ADDRESS(ES)</b> NASA Langley Research Center Hampton, VA 23681-0001			<b>8. PERFORMING ORGANIZATION REPORT NUMBER</b>	
<b>9. SPONSORING / MONITORING AGENCY NAME(S) AND ADDRESS(ES)</b> National Aeronautics and Space Administration Washington, DC 20546-0001			<b>10. SPONSORING / MONITORING AGENCY REPORT NUMBER</b> NASA TM-109093	
<b>11. SUPPLEMENTARY NOTES</b> Blanchard: Langley Research Center, Hampton, VA; Nicholson: ViGYAN, Inc., Hampton, VA; and Ritter and Larman: Lockheed Engineering and Sciences Co., Hampton, VA.				
<b>12a. DISTRIBUTION / AVAILABILITY STATEMENT</b> Unclassified - Unlimited  Subject Category 19			<b>12b. DISTRIBUTION CODE</b>	
<b>13. ABSTRACT (Maximum 200 words)</b> The Orbital Acceleration Research Experiment (OARE), which has flown on STS-40, STS-50 and STS-58, contains a three axis accelerometer with a single, non-pendulous, electrostatically suspended proofmass which can resolve accelerations to the nano-g (10 <sup>-9</sup> g) level. The experiment also contains a full calibration station to permit <i>in situ</i> bias and scale factor calibration. This on-orbit calibration capability eliminates the large uncertainty of ground-based calibrations encountered with accelerometers flown in the past on the Orbiter, thus providing absolute acceleration measurement accuracy heretofore unachievable. This is the first time accelerometer scale factor measurements have been performed on orbit. A detailed analysis of the calibration process is given along with results of the calibration factors from the on-orbit OARE flight measurements on STS-58. In addition, the analysis of OARE flight maneuver data used to validate the scale factor measurements in the sensor's most sensitive range is also presented. Estimates on calibration uncertainties are discussed. This provides bounds on the STS-58 absolute acceleration measurements for future applications.				
<b>14. SUBJECT TERMS</b> Orbital Acceleration Research Experiment (OARE), accelerometer, and Orbiter			<b>15. NUMBER OF PAGES</b> 52	
			<b>16. PRICE CODE</b> A04	
<b>17. SECURITY CLASSIFICATION OF REPORT</b> Unclassified	<b>18. SECURITY CLASSIFICATION OF THIS PAGE</b> Unclassified	<b>19. SECURITY CLASSIFICATION OF ABSTRACT</b>	<b>20. LIMITATION OF ABSTRACT</b>	





3 1176 01408 6459

**DO NOT REMOVE SLIP FROM MATERIAL**

Delete your name from this slip when returning material to the library.

NAME	DATE	MS
William Grantham	12-29-94	161